Stem Cell Reports
Article

ISSCR

OPEN ACCESS

Genetic Activation of Hedgehog Signaling Unbalances the Rate of Neural Stem Cell Renewal by Increasing Symmetric Divisions

Julien Ferent,[1] Loïc Cochard,[1] Hélène Faure,[1] Maurizio Taddei,[2] Heidi Hahn,[3] Martial Ruat,[1,4,*] and Elisabeth Traiffort[1,4,*]

[1]Laboratory of Neurobiology and Development-CNRS, Signal Transduction and Developmental Neuropharmacology Team, Institute of Neurobiology Alfred Fessard, Gif-sur-Yvette 91198, France
[2]Dipartimento Farmaco Chimico Tecnologico, Università degli Studi di Siena, 53100 Siena, Italy
[3]Tumor Genetics Group, Institute of Human Genetics, University Medical Center, Göttingen 37073, Germany
[4]Co-senior author
*Correspondence: ruat@inaf.cnrs-gif.fr (M.R.), elisabeth.traiffort@inserm.fr (E.T.)
http://dx.doi.org/10.1016/j.stemcr.2014.05.016

SUMMARY

In the adult brain, self-renewal is essential for the persistence of neural stem cells (NSCs) throughout life, but its regulation is still poorly understood. One NSC can give birth to two NSCs or one NSC and one transient progenitor. A correct balance is necessary for the maintenance of germinal areas, and understanding the molecular mechanisms underlying NSC division mode is clearly important. Here, we report a function of the Sonic Hedgehog (SHH) receptor Patched in the direct control of long-term NSC self-renewal in the subependymal zone. We show that genetic conditional activation of SHH signaling in adult NSCs leads to their expansion and the depletion of their direct progeny. These phenotypes are associated in vitro with an increase in NSC symmetric division in a process involving NOTCH signaling. Together, our results demonstrate a tight control of adult neurogenesis and NSC renewal driven by Patched.

INTRODUCTION

Neural stem cells (NSCs) remain in specialized niches of the brain over the lifespan and give rise to new neurons that integrate neural circuits. They are proposed to enable regeneration of injured tissue. The subependymal zone (SEZ), one of the main neurogenic niches in the adult mammalian brain, is comprised of astrocyte-like NSCs corresponding to a heterogeneous cell population. Among the identified subpopulations, active NSCs (aNSCs) expressing the epidermal growth factor receptor (EGFR) give rise to transit amplifying progenitors (TAPs). Most of these cells generate neuroblasts, migrating along the rostral migratory stream (RMS) and differentiating into granule and periglomerular interneurons in the olfactory bulb (OB). Quiescent NSCs (qNSCs) do not express the EGFR and are resistant to antimitotic drugs or irradiation. They are implicated in SEZ neurogenesis replenishment through aNSCs and TAPs (Costa et al., 2011; Pastrana et al., 2011; Ponti et al., 2013). Establishing the identity and lineage of SEZ stem cells is under intense studies, but the regulatory mechanisms involved in their self-renewal and differentiation still need more investigation. Only a few signals determining these distinct behaviors have been discovered. For instance, bone morphogenetic protein signals and EGFR-mediated inactivation of NOTCH signaling in NSCs are required for progression of the NSC progeny toward the neurogenic lineage (Aguirre et al., 2010; Colak et al., 2008), whereas the pigment epithelium-derived factor was proposed to regulate the NSC expansion (Karpowicz et al., 2009).

The Sonic Hedgehog (SHH) pathway is active in the adult SEZ, where it has been proposed to regulate cell proliferation (Ruat et al., 2012; Ahn and Joyner, 2005; Machold et al., 2003) and to modulate the migration of neuroblasts exiting the niche (Angot et al., 2008). The mosaic inactivation of the Smoothened (SMO) receptor in cell types expressing the neuroepithelial marker NESTIN suggested the requirement of this transducer of SHH signal for maintenance of the NSC population (Balordi and Fishell, 2007). Patched (PTC) is the main SHH receptor and is considered an antagonist of the pathway (Briscoe and Thérond, 2013). Embryonic deletion of *Ptc* in multipotent stem cells of human glial fibrillary acidic protein (hGFAP)-*Cre;Ptc*$^{C/C}$ mice results in medulloblastoma. The tumors do not manifest until the cells have committed to the neuronal lineage (Yang et al., 2008). However, the effects of *Ptc* inactivation in adult NSCs of the SEZ remain yet unknown.

Here, we used a tamoxifen-inducible Cre transgene under the control of the astrocyte-specific glutamate transporter (GLAST) expressed in astrocyte-like NSCs (Mori et al., 2006) and took advantage of a conditional *Ptc* knockout (*Ptc*$^{fl/fl}$) mouse line that has loxP recombinase recognition sites within the *Ptc* gene (Uhmann et al., 2007). We show that *Ptc* inactivation in the adult NSCs leads to a dramatic decrease of the neurogenic process and to a marked expansion of NSCs in the SEZ. Neurogenesis blockade was related to a shift in NSC division mode from asymmetric to symmetric, leading to a decrease in the differentiation process and involving NOTCH

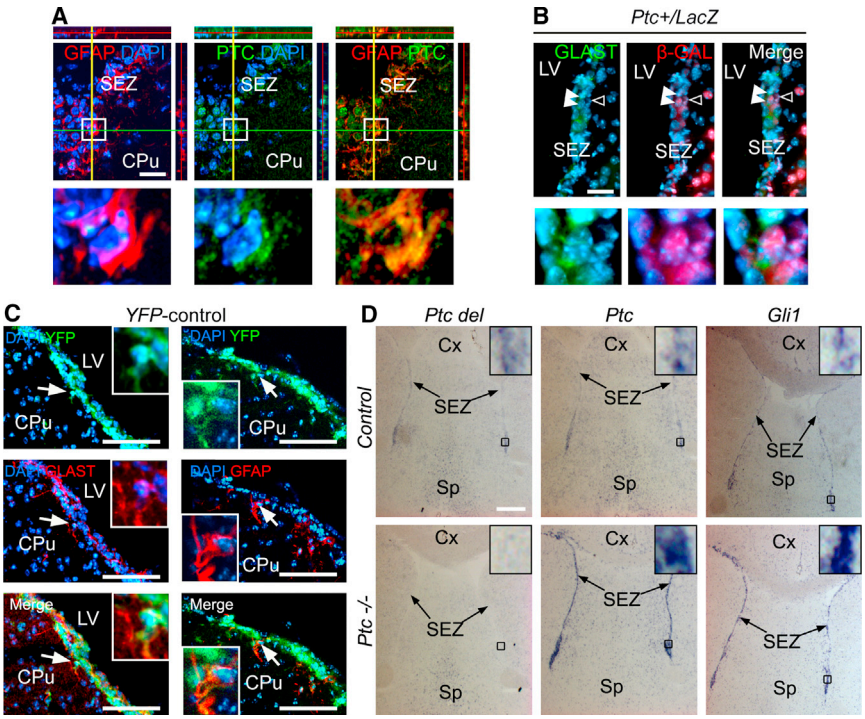

Figure 1. Inducible Deletion of *Ptc* in GLAST-Expressing Cells from the Adult Brain SEZ

(A) Immunohistofluorescence (IHF) indicating the presence of a population of PTC$^+$ cells (green) coexpressing the astroglial marker GFAP (red) in the dorsal SEZ. Magnifications of the boxed areas are presented below each panel.

(B) Double IHF performed on brain slices from the heterozygous *Ptc*$^{+/LacZ}$ mouse that expresses the LACZ reporter in one allele of *Ptc*. Anti-β-GAL (red) and GLAST (green) antibodies are used. Magnifications of the area indicated by arrowheads are presented below each panel and show β-GAL$^+$ nuclei surrounded (white arrowheads) or not (black and white arrowhead) by GLAST$^+$ signal.

(C) Fluorescent signals of YFP together with GLAST and GFAP in the SEZ of *Glast-CreERT2;R26R-YFP* (YFP-control) mice 2 months after tamoxifen administration. The white arrow indicates a cell coexpressing YFP with alternatively GLAST or GFAP markers and magnified in the inset. Nuclei are in blue (DAPI) in (A)–(C).

(D) In situ hybridization (ISH) of two HH target genes, *Ptc* and *Gli1*, in the SEZ of mice in which *Ptc* exons 8 and 9 are flanked by loxP sites. In *Ptc*$^{-/-}$ (*Glast-CreERT2;Ptc*$^{fl/fl}$) mice, exons 8 and 9 were depleted by tamoxifen-mediated activation of *Glast-CreERT2* that is expressed from the endogenous *Glast* locus. Tamoxifen-treated *Ptcfl/fl* mice served as controls (control). Two months after tamoxifen treatment, the animals were subjected to analysis. The *Ptc del* riboprobe encompasses nucleotides of *Ptc* exons 8 and 9 and thus detects only the WT *Ptc* transcripts. The *Ptc* riboprobe corresponds to half of the full-length *Ptc* transcript, including the C-terminal end. In the control mice, *Ptc del*, *Ptc*, and *Gli1* allow the detection of the faint labeling previously reported in the SEZ with a stronger signal in the ventral niche. In *Ptc*$^{-/-}$ mice, strong *Ptc* and *Gli1* signals are detected in the ventral and dorsal SEZ, whereas no signal is observed when the *Ptc del* riboprobe is used.

CPu, caudate putamen; Cx, cerebral cortex; LV, lateral ventricle; Sp, septal area. Scale bars, 50 μm (A and B), 100 μm (C), and 200 μm (D). See also Figures S1 and S2.

signaling. Thus, we report a role for PTC in the regulation of adult NSC self-renewal mechanisms.

RESULTS

Conditional Deletion of *Ptc* in GLAST-Expressing Cells Promotes Endogenous Activation of HH Signaling in the SEZ Niche

To investigate the role of PTC in NSCs of the adult SEZ niche, we used a genetic approach aimed at conditionally deleting this receptor in the astroglial population in which we formerly demonstrated its expression (Figure 1; Figure S1 available online). *Ptc* transcripts and proteins were evidenced in the SEZ niche. Confocal analysis using a specific PTC antiserum (Bidet et al., 2011; Figure S1) showed PTC expression in a subset of GFAP$^+$ cells (36% ± 5%) (Figure 1A). Moreover, analysis of the *Ptc*$^{+/LacZ}$ mice (Goodrich et al., 1997) led to visualizing β-galactosidase (β-GAL$^+$)/PTC$^+$ cells coexpressing GLAST, a marker of astrocyte-like NSCs (Figure 1B). Therefore, we took advantage of the *Glast-CreERT2* mouse line (Mori et al., 2006) expressing a tamoxifen-inducible *Cre* in the locus of *Glast* to induce Cre recombinase activity specifically in adult astroglia and NSCs. *Glast-CreERT2* mice were crossed with the *Rosa26* reporter line, *R26R-YFP* (yellow fluorescent protein) (Srinivas et al., 2001). In the *Glast-CreERT2;Ptc*$^{WT/WT}$*;R26R-YFP* offspring (so-called *YFP*-control), YFP expression is initiated upon tamoxifen-mediated activation of the Cre recombinase and permanently marks all progeny of the recombined cells. At 2 months after tamoxifen treatment, a high number of YFP$^+$ cells are detected in the SEZ that coexpress the astrocyte markers GLAST and GFAP (Figure 1C). Confocal analysis of the SEZ niche indicated that YFP reporter is expressed in 85% ± 5% of GLAST$^+$ cells. Recombination also occurred in neurogenic astroglial-like cells of the hippocampal subgranular zone and in other astrocyte

populations throughout the brain as expected from *Glast* expression profile (Mori et al., 2006) (Figure S2A).

Ptc was inactivated in GLAST$^+$ cells by crossing alternatively the *Glast-CreERT2* or *YFP*-control with *Ptc*$^{fl/fl}$ mouse lines allowing the excision of exons 8 and 9 encoding a domain involved in SHH binding (Uhmann et al., 2007). Adult *Glast-CreERT2;Ptc*$^{fl/fl}$ (so-called *Ptc*$^{-/-}$) mice and littermate *Ptc*$^{fl/fl}$ controls (so-called control) were treated with tamoxifen and analyzed 10 days, or 2, 6, or 12 months later. Despite a loss of body weight in *Ptc*$^{-/-}$ animals treated with tamoxifen 1 year before, their brain was macroscopically indistinguishable from the brain of the controls. Notably, no tumor could be detected (data not shown). Analyses of *Gli1* or *Ptc* transcription were used as readouts of Hedgehog (HH) pathway activation (Briscoe and Thérond, 2013). In *Ptc*$^{-/-}$ mice, both genes were highly upregulated in ventral and dorsal SEZs, indicating a sustained activation of HH signaling compared to controls. Additional control experiments demonstrated the specificity of both *Gli1* and *Ptc* transcription in *Ptc*$^{-/-}$ animals (Figure 1D; see Figures S2B and S2C). Altogether, these results demonstrate that Cre-mediated recombination allows the efficient deletion of *Ptc* in GLAST$^+$ cells, leading to the persistent activation of HH signaling in the adult SEZ niche.

Ptc Deletion Affects Both Fast and Slow Proliferation and Decreases Neurogenesis

To determine the functional meaning of *Ptc* deletion in GLAST$^+$ cells in the SEZ, we first examined fast proliferating cells (TAPs and neuroblasts) by administrating to the animals two bromodeoxyuridine (BrdU) pulses at 2 hr intervals. Pulsing was done at various time points (10 days, and 2, 6, and 12 months) after tamoxifen injection. The animals were sacrificed after the last BrdU pulse (Figures 2A and 2B). In control animals, BrdU$^+$ cell number decreases between 2 and 6 months after treatment, presumably reflecting a regular decline associated with aging as previously shown by Shook et al. (2012). Interestingly, BrdU$^+$ cells were significantly decreased in the SEZ of *Ptc*$^{-/-}$ mice when compared to controls over the course of the study. At 10 days, the 27% decrease was already highly significant and reached 54% at 2 months. The drop in fast proliferating cells was still observed after 6 months and led to their almost complete disappearance at 1 year in *Ptc*$^{-/-}$ animals, likely related to both the observed phenotype and the regular decrease occurring in aging. We excluded cell survival decrease because the number of terminal deoxynucleotidyl transferase dUTP nick end labeling-positive cells was not significantly modified in *Ptc*$^{-/-}$ SEZs over the course of the study (Figure S3). Remarkably, the SEZ visualization of EGFR$^+$ cells corresponding to TAPs and a low percentage of transitional stages (Pastrana et al., 2011; Ponti et al., 2013) revealed a dramatic 93% decrease of this cell population at 12 months in the *Ptc* mutants (Figures 2C and 2D). Polysialylated-neuronal cell adhesion molecule (PSA-NCAM$^+$)-positive cell number was reduced by more than 90% in *Ptc*$^{-/-}$ mice, which is consistent with a high rate of *Ptc* excision in these animals, resulting in the quite complete absence of SEZ-migrating neuroblasts (Figures 2C and 2D). In contrast, the density of *Gfap*$^+$ cells that correspond to astrocytes and NSCs in the SEZ showed a robust 62% increase in *Ptc*$^{-/-}$ animals analyzed at 12 months (Figures 2E and 2F).

Consistently, at 2 months, quantification of SEZ cell populations indicated that the *Ptc* deletion increases by almost 2-fold the number of GLAST$^+$ cells corresponding to both niche astrocytes and NSCs, and the number of KI67$^+$/GFAP$^+$ NSCs. TAPs and neuroblasts were decreased by 2-fold as indicated by EGFR and PSA-NCAM stainings (Figures 2G and 2H). Moreover, in the absence of *Ptc*, we found a marked increase in the number of sex-determining region Y-box 2$^+$ (SOX2$^+$) and SOX9$^+$ cells both expressed in NSCs and TAPs (Kazanis et al., 2010; Scott et al., 2010). Because the TAP population is reduced, the increase in SOX2$^+$ and SOX9$^+$ cells may consistently reflect the increase of NSC density. Together, these data show that the *Ptc* deletion is thus associated with an increase in the number of astrocyte-like NSCs in the SEZ and a decrease in the number of TAPs and migrating neuroblasts.

The progeny of the recombined cells was traced by following the expression of YFP in *Glast-CreERT2;Ptc*$^{fl/fl}$*;R26R-YFP* (so-called *YFP-Ptc*$^{-/-}$) and *YFP*-control mice treated with tamoxifen and analyzed 2 months later. As expected, strong YFP signals were detected in the SEZ-RMS-OB system of *YFP*-control mice (Figure 3A) and also in the corpus callosum (cc), where they reflect both the population of newly generated oligodendroglial cells derived from the SEZ (Gonzalez-Perez and Alvarez-Buylla, 2011) and the local GLAST-expressing astroglial cells present in the fiber tracts (Figure S4A). In *YFP-Ptc*$^{-/-}$ animals, YFP expression level was dramatically affected except in the SEZ, where the density of YFP$^+$ cells was only slightly reduced without reaching significance (Figure 3B). The apparent divergence between the unaltered YFP$^+$ cell density and the substantial reduction in the number of BrdU$^+$ cells in the SEZ may be explained for the former by a compensatory mechanism between the increase in NSCs and the decrease in TAPs/neuroblasts and for the latter by the collapse of the dynamics of TAPs and neuroblasts. Indeed, TAPs have been proposed to divide three times before turning into neuroblasts and neuroblasts once or twice before leaving the SEZ (Ponti et al., 2013). In *YFP-Ptc*$^{-/-}$ animals, quantification of YFP$^+$ cells in the OB granular (GrO) and glomerular (Gl) layers (Figure 3B; see also Figures S4A–S4C) and in the cc (Figures S4D–S4F) indicated a 69%, 36%, and 51% decrease, respectively. Interestingly,

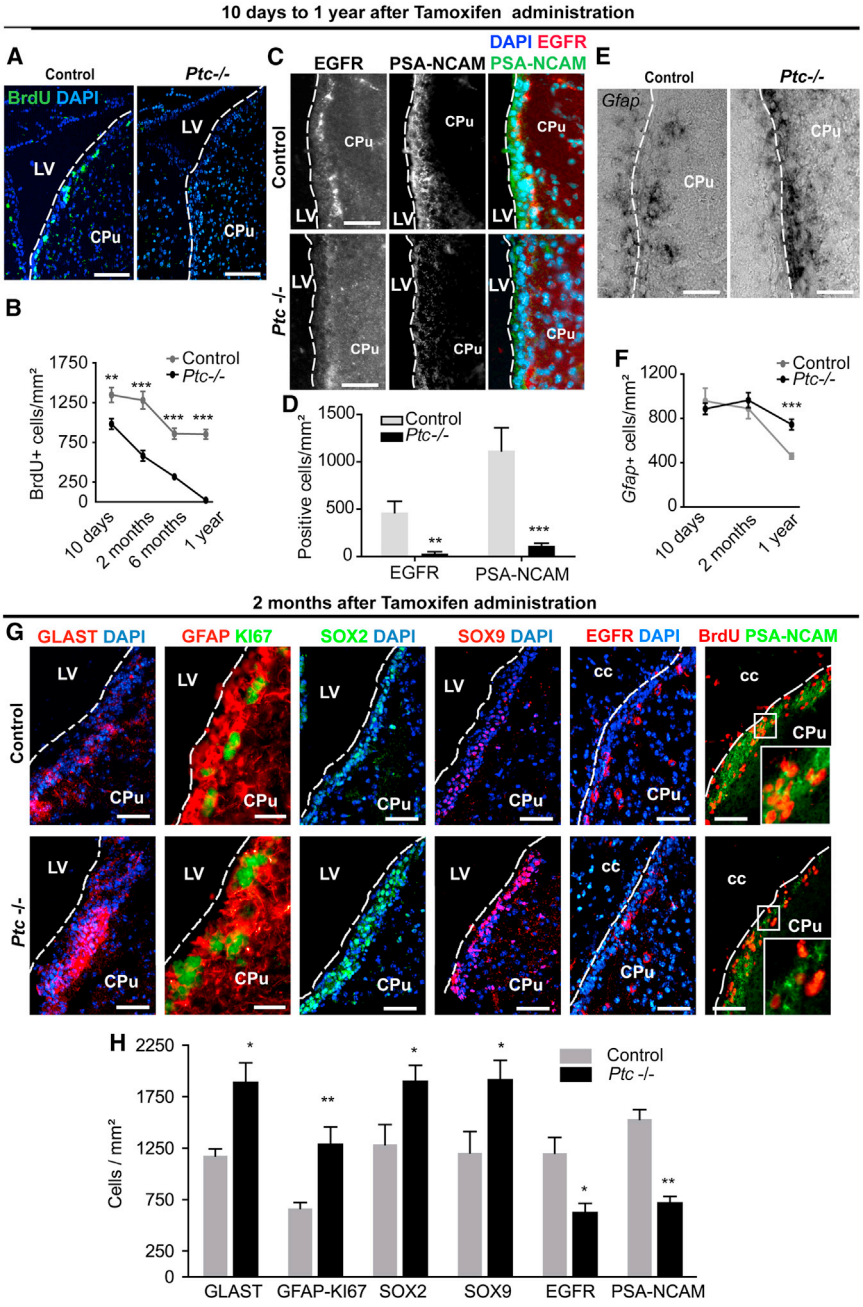

Figure 2. Alteration of Cell Proliferation and Phenotype in the Adult SEZ/RMS upon *Ptc* Deletion

(A) Detection of fast proliferating cells by IHF using anti-BrdU antibody in brain slices of $Ptc^{-/-}$ and control animals treated 1 year before with tamoxifen and analyzed 2 hr after short BrdU pulses.

(B) Histogram depicting the number of $BrdU^+$ and $GFAP^+$ cells quantified in the SEZ at the indicated time after tamoxifen treatment.

(C and D) IHF visualizing the expression of EGFR (red) and PSA-NCAM (green) in the SEZ of control and $Ptc^{-/-}$ mice 1 year after tamoxifen administration and quantification.

(E and F) ISH showing the *Gfap* gene expression in the SEZ of control and $Ptc^{-/-}$ mice 1 year after tamoxifen administration and quantification for the various time points.

(G) Fluorescent micrographs in the adult SEZ of control and $Ptc^{-/-}$ mice 2 months after tamoxifen administration. The micrographs depict immunostainings for GLAST and GFAP/KI67 as astrocyte and stem cell markers, SOX2 and SOX9 as transcription factors necessary for NSC formation, and EGFR and PSA-NCAM as markers of TAPs and migrating neuroblasts, respectively. In the last panels, BrdU labels the fast proliferating cell populations. The dashed lines delineate the wall of the lateral ventricle except for the last two panels on the right where they delineate the cc.

(H) Histograms describing the number of each cell type per square millimeter. Values are the mean ± SEM from three to four animals, two to four slices per animal.

CPu, caudate putamen; LV, lateral ventricle. $*p \leq 0.05$; $**p \leq 0.005$; $***p \leq 0.0005$. Scale bars, 100 μm (A and G), 25 μm (GFAP/KI67 pictures in G), and 50 μm (C and E). See also Figure S3.

in the granular layer, YFP^+ cells are decreased in both deep and superficial layers with, however, a slightly higher decrease in the deep layer. Thus, *Ptc* deletion affects both the ventral and dorsal parts of the SEZ known to contribute to the production of deep and superficial granule cells, respectively. This suggests that SHH signaling displays a broader effect than initially proposed alongside the whole SEZ (Ihrie et al., 2011). Moreover, the fluorescent signal was also dramatically reduced in the RMS connecting the SEZ to the OB (Figure 3A).

Because these results indicated a decrease in the generation of new cells in the SEZ, we further analyzed the phenotype of SEZ-derived cells at their final destinations: the OB (Figures 3C and 3D), and the cc (Figure S4C). In the GrO layer of the OB where the newly generated cells mature as GABAergic interneurons, the percentage of YFP^+ cells expressing the neuronal marker NEUN or C-FOS, a transcription factor rapidly regulated by neuronal activity, was unchanged in $Ptc^{-/-}$ mice. These data indicated that there was no difference in the proportion of neurons fully

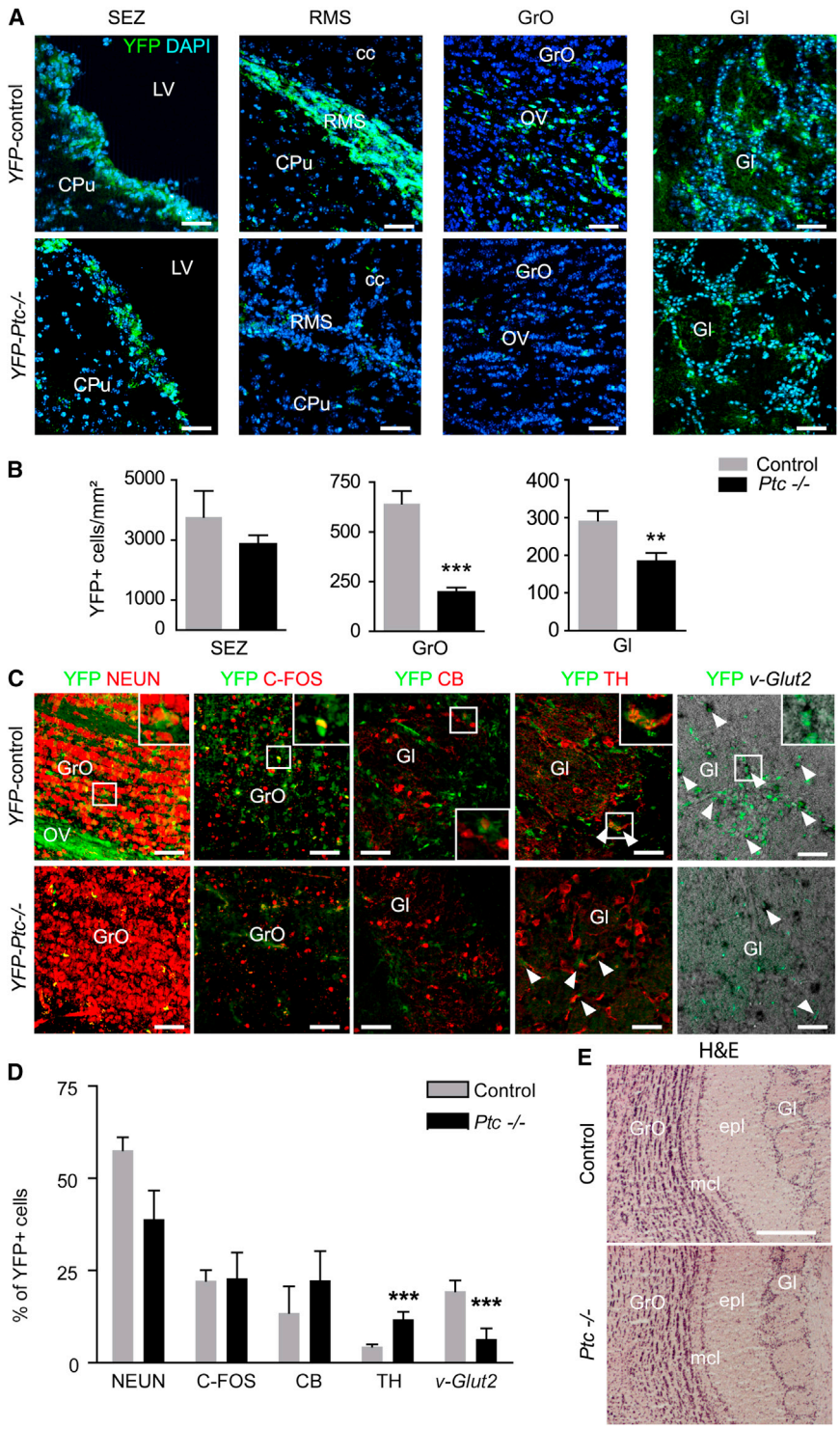

Figure 3. Cell Fate Analysis after Deletion of *Ptc* in the Adult SEZ

(A) Tracing of *Glast*$^+$ cells in *YFP-Ptc*$^{-/-}$ and *YFP*-control mice treated with tamoxifen 2 months before. YFP is detected in the SEZ, RMS, and OB. A lower density of YFP$^+$ cells is observed in the RMS and OB of *YFP-Ptc*$^{-/-}$ mice compared to *YFP*-controls. In contrast, no difference is observed in the SEZ.

(B) Quantification of the density of YFP$^+$ cells in the SEZ and OB layers.

(C) Phenotype of the targeted cells at their final destination upon conditional *Ptc* deletion in the SEZ. IHF (NEUN, C-FOS, CB, and TH) or ISH (*v-Glut2*) in slices from *YFP*-control or *YFP-Ptc*$^{-/-}$ mice at the level of the OB is shown. White arrowheads indicate double-labeled cells.

(D) Histogram presenting the percentage of each cell phenotype within the YFP population.

(E) Brain slices performed at the level of the OB from control and *Ptc*$^{-/-}$ mice treated with tamoxifen 1 year before and stained with hematoxylin and eosin (H&E). No alteration of the multilayered cellular architecture of the OB is observed. Values are the mean ± SEM from three to four animals, two to four slices per animal.

$^{**}p \leq 0.005$; $^{***}p \leq 0.0005$. Scale bars, 50 μm (A and C) and 200 μm (E).

See also Figure S4.

integrated into the GrO layer. We then analyzed the percentage of YFP$^+$ cells expressing tyrosine hydroxylase (TH), calbindin, or vesicular glutamate transporter 2 (*vGlut2*), which labels subsets of SEZ-derived new cells integrating the Gl layer (Brill et al., 2009). In the conditional *Ptc* mutants, the percentage of newly generated calbindin$^+$ cells was not significantly modified. In contrast, the percentages of YFP$^+$ cells coexpressing either TH or *vGlut2* were 3-fold higher or lower, respectively. Remarkably, at 1 year post tamoxifen, the multilayered cellular

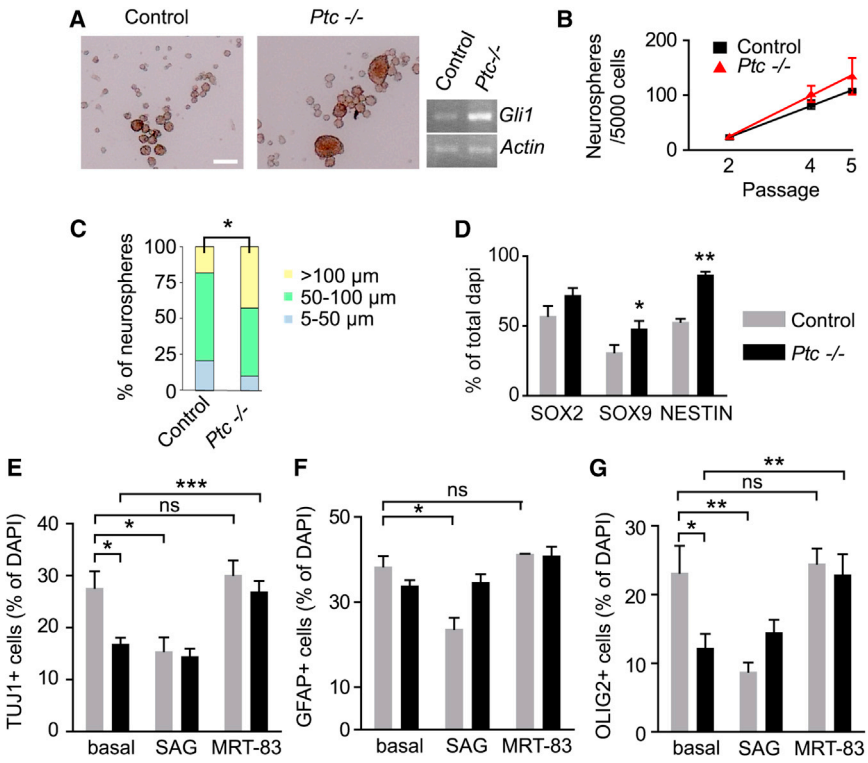

Figure 4. Sustained HH Signaling Activation in SEZ-Derived Neural Progenitors Maintains NSC Multipotency in the Neurosphere Assay

(A and B) SEZ neurospheres derived from $Ptc^{-/-}$ mice analyzed 2 months after tamoxifen administration can be expanded in a similar manner as controls and display *Gli1* upregulation. The neurosphere numbers obtained at each passage were analyzed via a linear regression model. The rate of clonal expansion is represented as the slope of the lines ($Ptc^{-/-}$ 0.256 ± 0.047 versus control 0.226 ± 0.016; $p > 0.05$).

(C) Large sphere number (>100 µm in diameter) is slightly, but significantly, higher in $Ptc^{-/-}$ compared to controls ($p = 0.03$). Values are expressed as the percentage of the total number of spheres generated from 5,000 plated cells (total counted spheres: n = 138 for $Ptc^{-/-}$, n = 98 for controls).

(D) Evaluation of the expression of progenitor cell markers (SOX2, SOX9, and NESTIN) in cells dissociated from neurospheres and then cultured for 12 hr in the absence of growth factors. Quantification of each cell type indicates a significant increase in the number of $SOX9^+$ and $NESTIN^+$ cells. The mean numbers of counted cells per marker are 227 ± 67 and 356 ± 147 for $Ptc^{-/-}$ and controls, respectively.

(E–G) Histograms depicting the differentiation potential of neurospheres from $Ptc^{-/-}$ and control mice cultured for 7 days without growth factors in the absence or the presence of pharmacological HH modulators, including the SMO agonist SAG (0.3 µM) and antagonist MRT-83 (3 µM). Differentiated cells were analyzed by IHF using TUJ1, GFAP, and OLIG2 antibodies to characterize neuronal (E), astroglial (F), and oligodendroglial (G) cells, respectively. In the absence of drugs, a significant decrease in the percentage of $TUJ1^+$ and $OLIG2^+$ cells is observed in $Ptc^{-/-}$ compared to control cells. The mean numbers of counted cells for each marker are 1,699 ± 309 and 3,822 ± 128 for $Ptc^{-/-}$ and controls, respectively. The data are expressed as the mean ± SEM of the percentage of $DAPI^+$ nuclei, which express each marker and are derived from three independent experiments.

*$p \leq 0.05$; **$p \leq 0.01$; ***$p \leq 0.005$; ns, nonsignificant. Scale bar, 100 µm.

See also Figure S5.

architecture of the OB was not altered in $Ptc^{-/-}$ compared to control (Figure 3E). In the cc, a 2-fold lower proportion of YFP^+ cells expressing OLIG2 was observed in *YFP-*$Ptc^{-/-}$ animals (Figure S4C), suggesting that *Ptc* deletion decreases the ability of precursor cells to give rise to oligodendrocytes. As a whole, these data establish that the generation of new precursors is highly decreased in the SEZ of the conditional *Ptc* mutants. Although these precursors still have the ability to differentiate into neurons and oligodendrocytes in the OB and cc, respectively, they nevertheless display discrete variations of fate determination.

Ptc Deficiency in SEZ-Derived Neural Progenitors Changes Cell Differentiation Capacity in the Neurosphere Assay

To address the consequences of *Ptc* deficiency in SEZ progenitors, we used the neurosphere culture to analyze stem and progenitor cell properties between *Ptc*-deficient and control cells (Pastrana et al., 2011). We observed no difference in sphere formation of cells derived from $Ptc^{-/-}$ SEZs 2 months after tamoxifen injection, despite *Gli1* upregulation observed in *Ptc*-deficient neurospheres (Figures 4A and 4B). The clonal expansion represented as the slope of the line indicated that *Ptc* deficiency does not alter the apparent capacity of self-renewal of the neurospheres. However, when we quantified the subpopulations of neurospheres according to their diameter, we observed a higher number of large neurospheres (≥100 µm) derived from the $Ptc^{-/-}$ SEZ (Figure 4C). This observation may suggest that more stem cells are present in *Ptc*-deficient spheres because it was previously proposed that aNSCs give rise to large spheres, whereas progenitors lead to smaller ones (Pastrana et al., 2011). This is also consistent with a decrease in TAPs in the SEZ of these animals as previously observed.

When dissociated neurospheres were cultured for 12 hr in the absence of growth factors, significantly more cells were positive for SOX9 in the *Ptc*-deficient neurospheres when compared to the controls (Figure 4D; see also Figure S5A), consistent with our in vivo data and also with the upregulation of SOX9 observed upon HH activation (Scott et al., 2010). In contrast, SOX2 expression did not significantly differ between the groups, whereas the number of NESTIN$^+$ neuroepithelial cells was increased by 1.6-fold, indicating that the *Ptc* deficiency has inhibited differentiation. To further evaluate the multipotency of *Ptc*$^{-/-}$ NSCs, the neurospheres were cultured for 7 days in the absence of growth factors to allow differentiation into neurons, oligodendrocytes, and astrocytes. Although *Ptc*$^{-/-}$ NSCs maintain their multipotency, their ability to differentiate was modified (Figures 4E–4G; see also Figure S5B). The percentage of TUJ1$^+$ neuroblasts and OLIG2$^+$ oligodendrocytes (only OLIG2$^+$ GFAP$^-$ cells were counted to avoid including immature OLIG2$^+$ GFAP$^+$ astrocytes as previously reported in Marshall et al., 2005) was significantly reduced in *Ptc*-deficient cells, whereas the number of GFAP$^+$ astrocytes was not modified by the *Ptc* deletion. Then, we addressed the question whether the effects observed above in *Ptc*-deficient cells could be modulated through SMO (Figures 4E–4G). In agreement with the involvement of SMO activation in *Ptc*$^{-/-}$ phenotype, the number of TUJ1$^+$ neuroblasts, OLIG2$^+$ oligodendrocytes, and GFAP$^+$ astrocytes was reduced in cells derived from control mice upon addition of Smoothened agonist (SAG), a reference SMO activator (Chen et al., 2002). In contrast, application of the SMO antagonist MRT-83 (Roudaut et al., 2011) did not modify the generation of any cell types, suggesting that HH signaling is already antagonized by PTC. However, application of MRT-83 increased the capacity of *Ptc*$^{-/-}$ cells to differentiate into neuroblasts, oligodendrocytes, and astrocytes. Thus, the rescue of the *Ptc*$^{-/-}$ phenotype by SMO blockade is likely associated with the relief of PTC constitutive inhibitory effect on SMO. Importantly, *Ptc* deficiency decreases the total number of cells reaching the differentiated state, although it does not prevent cells from achieving terminal multilineage differentiation.

Ptc Deficiency in SEZ-Derived Neural Progenitors Promotes Symmetric GLAST$^+$/EGFR$^-$ NSC Pairs through NOTCH Signaling and Reduces Cell-Cycle Exit of TAPs

The inactivation of *Ptc* in GLAST$^+$ cells in the adult SEZ resulting in an increase of NSCs prompted us to investigate the potential crosstalk between HH and NOTCH signaling, which has been shown to regulate cell cycle to balance NSC maintenance during corticogenesis (Dave et al., 2011) and to be essential for the maintenance of NSCs (Aguirre et al., 2010; Imayoshi et al., 2013). First, we used the clonal pair cell assay adapted from the previously described protocol of Dave et al. (2011). We plated primary cells directly after their isolation from the SEZ, and we maintained them in culture 24–36 hr to allow cell division. We used GLAST and EGFR antibodies to label the stem cells and their direct progeny, respectively. SEZ-derived cells isolated from wild-type (WT) mice were treated with the SMO agonist SAG in the presence or absence of the inhibitor of γ-secretase, LY411575, which suppresses proteolysis-dependent activation of endogenous NOTCH receptors (Fauq et al., 2007). SAG significantly promotes symmetric GLAST$^+$/EGFR$^-$ pairs at the expense of GLAST$^+$/EGFR$^+$ pairs compared to the basal condition. The SAG-mediated effect was counteracted by LY411575 treatment as well as by the SMO antagonist MRT-83 (Figures 5A and 5B). This indicates that HH-dependent generation of symmetric GLAST$^+$/EGFR$^-$ pairs, likely corresponding to an activated state of NSCs different from those that are GLAST$^+$/EGFR$^+$, is also NOTCH dependent. Then, we performed semiquantitative RT-PCR analysis in SVZ-derived neurospheres from conditional *Ptc*$^{-/-}$ and control animals treated with tamoxifen for 2 months. *Notch1* and two of its canonical effectors, the transcription factors *Hes1* and *Hes5* (Imayoshi et al., 2013), are upregulated when *Ptc* is conditionally deleted (Figure 5C). These data indicate that the NOTCH signaling pathway is activated upon *Ptc* deletion.

We next tested if the above-reported effect on symmetric GLAST$^+$/EGFR$^-$ NSCs observed upon pharmacological activation of SMO could be observed upon genetic deletion of *Ptc* in the adult NSCs. In cell cultures derived from *Ptc*$^{-/-}$ mice that received a tamoxifen injection 2 months before, a 4- to 5-fold increase of symmetric GLAST$^+$/EGFR$^-$ pairs was detected at the expense of both the asymmetric pairs and symmetric GLAST$^+$/EGFR$^+$ pairs compared to the controls (Figures 5D and 5E). Thus, *Ptc* deficiency in adult SEZ-derived NSCs favors the generation of symmetric GLAST$^+$/EGFR$^-$ NSCs. The absence of significant decrease in the percentage of symmetric GLAST$^+$/EGFR$^+$ pairs suggests that the pharmacological activation of SMO in WT neurospheres is not fully comparable to the genetic deletion of *Ptc* regarding the mechanism of self-renewal of GLAST$^+$/EGFR$^-$ NSCs and aNSCs.

We determined the proportion of precursor cells labeled by a 2 hr pulse of BrdU in the population of cycling cells expressing KI67 in vivo in the SEZ of animals that received tamoxifen 2 months before. A 2 hr pulse of BrdU essentially reflects the proliferation of aNSCs, TAPs, and neuroblasts (Ponti et al., 2013). This protocol led us to determine that the labeling index was not modified by *Ptc* inactivation (Figures 5F and 5G). We also evaluated the number of cells exiting the cell cycle when animals were killed 24 hr after BrdU injection. The quantification of the number of

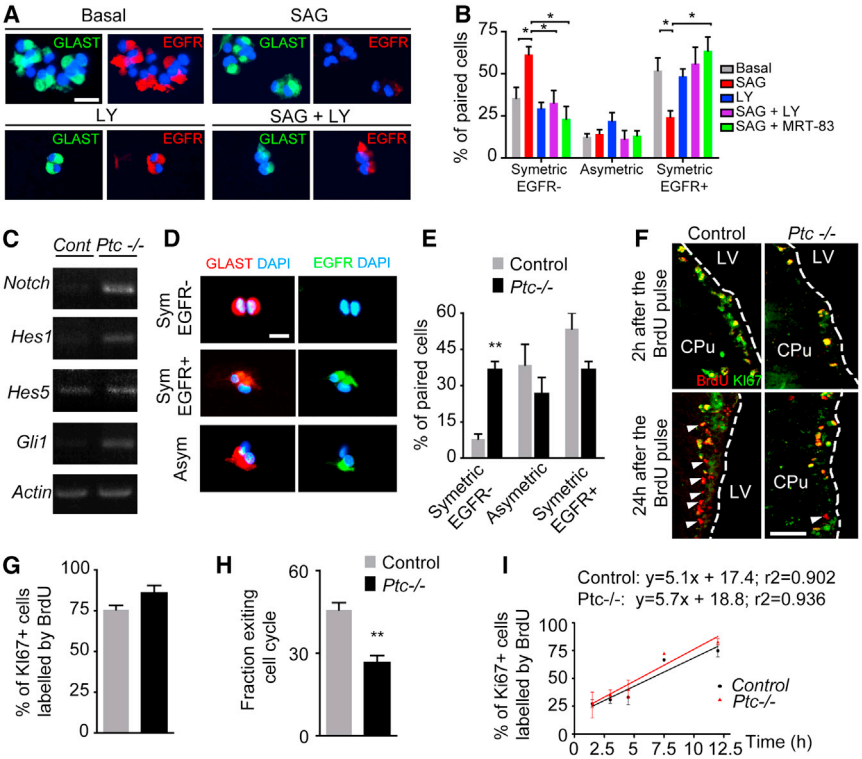

Figure 5. *Ptc* Deficiency Increases NSC Symmetric Division by Upregulating the NOTCH Pathway

(A) The clonal paired-cell assay is performed on SEZ-derived cells isolated from WT animals. The cells are cultured for 24–36 hr in the presence of the indicated drugs. SAG, LY, and MRT-83 were used at 0.3, 10, and 3 μM, respectively. The paired cells are labeled using GLAST (green) and EGFR (red) as markers of NSCs and TAPs, respectively. Nuclei are in blue (DAPI).

(B) Quantitative analysis of the percentage of each type of division indicates that SAG significantly increases the number of symmetric $GLAST^+/EGFR^-$ pairs compared to the basal condition. This effect is counteracted by treatments with the SMO and NOTCH antagonists, MRT-83 and LY, respectively. $^*p \leq 0.05$.

(C) The upregulation of *Gli1*, *Notch1*, and the NOTCH effectors *Hes1* and *Hes5* is detected by semiquantitative RT-PCR in SEZ-derived progenitors isolated from adult $Ptc^{-/-}$ mice when compared to control animals. *β-actin* was used to assess input RNA levels.

(D) The clonal paired-cell assay performed on SEZ-derived precursors isolated from adult $Ptc^{-/-}$ and control mice indicates that GLAST-expressing cells from $Ptc^{-/-}$ more frequently generate two $GLAST^+$ precursors after 24–36 hr when compared to control cultures.

(E) Quantitative analysis.

(F) BrdU (red) and KI67 (green) labeling of SEZ slices derived from $Ptc^{-/-}$ and control mice that had received tamoxifen 2 months before and were analyzed 2 or 24 hr after a single BrdU injection. The yellow fluorescence corresponds to double-labeled cells. In the bottom panels, the white arrowheads indicate the $BrdU^+KI67^-$ cells.

(G and H) The histograms show the percentage of $BrdU^+$ cells in the population of cycling cells 2 hr after the BrdU pulse (G) and the percentage of $BrdU^+$ cells that left the cell cycle ($KI67^-$) 24 hr after the BrdU pulse (H). Values are mean ± SEM from three to four animals, two to four slices per animal.

(I) Labeling index of cycling cells (i.e., the percentage of $KI67^+$ cells that have incorporated BrdU) in control and $Ptc^{-/-}$ SEZ-derived cells. The equations of the linear regressions for each group indicate no significant difference in the slopes and consequently similar cell-cycle lengths. For cell cultures, values are mean ± SEM from three experiments.

$^{**}p \leq 0.01$. Scale bars, 25 μm (A), 50 μm (D), and 100 μm (F). LY, LY411575.

proliferating cells remaining in the cell cycle 24 hr after BrdU incorporation (cells that are still $KI67^+$) showed that a nearly 2-fold lower percentage of *Ptc*-deficient cells exit the cell cycle when compared to the control (Figure 5H). By using the BrdU cumulative approach, we also addressed the question of a potential difference in the cell-cycle length of NSCs when *Ptc* is deleted. We cultured SEZ-derived cells from animals treated with tamoxifen 5 months earlier. Taking into account our in vivo results, at that time point, SEZ cells of $Ptc^{-/-}$ animals correspond to a majority of aNSCs because TAPs and neuroblasts have collapsed. Under such conditions, a shortening of cell-cycle length resulting in an increase in NSC proliferation should be clearly detected because aNSCs were reported to display the shortest cell-cycle length compared to neuroblasts and TAPs with values close to 17, 18, and 18–25 hr, respectively (Ponti et al., 2013). The cell-cycle length obtained in $Ptc^{-/-}$ culture is slightly but nonsignificantly shorter (14.2 hr) compared to the control cultures (16.2 hr), thus suggesting that the NSC proliferation is likely not increased (Figure 5I). Altogether, these data indicate that *Ptc* deficiency likely lowers the number of fast proliferating cells exiting the cell cycle and, thus, their ability to differentiate but does not increase aNSC proliferation in vitro.

PTC Is Required for Replenishment of the SEZ Stem Cell Niche after In Vivo AraC Treatment

Next, we examined in the SEZ of control and $Ptc^{-/-}$ animals treated with tamoxifen 6 months before, the fate of NSCs

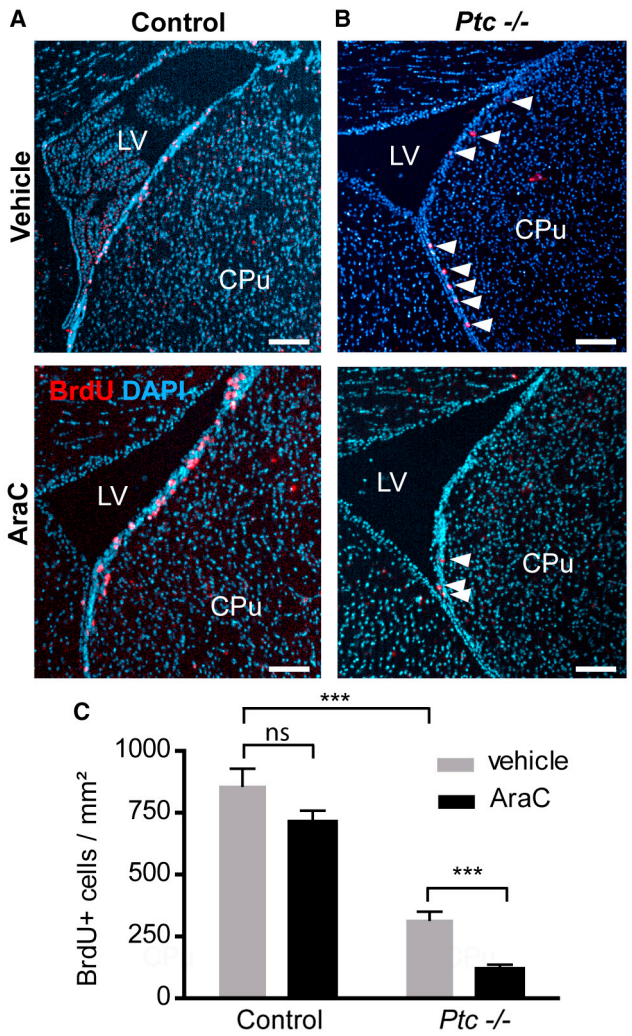

Figure 6. Altered Replenishment of the SEZ Stem Cell Niche in Conditional *Ptc*$^{-/-}$ Animals after AraC Injury In Vivo

(A and B) Coronal views of the SEZ showing BrdU-incorporating cells 10 days after pump removal in controls (A) and *Ptc*$^{-/-}$ (B) animals treated with vehicle or AraC. Animals had received tamoxifen 6 months before. The white arrowheads indicate BrdU^{+} nuclei. Scale bars, 100 μm.

(C) Quantification of BrdU-labeled cells in control and *Ptc*$^{-/-}$ animals. Values are the mean ± SEM from four animals/condition and two to four slices per animal. ***p ≤ 0.0001; ns, nonsignificant. See also Figure S6.

after an infusion with AraC, an antimitotic reagent that kills dividing NSCs, TAPs, and proliferating neuroblasts while sparing qNSCs. After transient impairment of neurogenesis by AraC treatment, the damaged SEZ is then regenerated by astrocyte-like NSCs resulting in the increase of cell proliferation and the production of aNSCs and TAPs (Pastrana et al., 2011). Immediately after AraC treatment (day 0), cells that incorporated BrdU were mostly missing, whereas 10 days later (day 10), BrdU^{+} cell population returned to normal in the control SEZ when compared to vehicle treatment (Figures 6A and 6C; see also Figure S6). However, the number of BrdU^{+} cells in the *Ptc*$^{-/-}$ SEZ was 3-fold lower after AraC compared to vehicle treatment (Figures 6B and 6C). These data indicate that, upon AraC treatment, *Ptc* deficiency prevents qNSCs to be activated and to give rise to TAPs. Thus, PTC is required for effective regeneration after lesion in the SEZ.

DISCUSSION

Conditional *Ptc* inactivation in the adult NSCs allowed the study of HH signaling activation in a ligand-independent, cell-intrinsic fashion in the SEZ in vivo. This activation is likely due to the suspension of the inhibitory effect of PTC on SMO and may promote the generation of symmetric GLAST^{+}/EGFR^{-} pairs as observed in vitro. Moreover, our data suggest a likely alteration of the transition from aNSCs to TAPs, which might account for the high decrease of TAPs and subsequently of neuroblasts. The expression of NOTCH signaling and high-mobility group box transcription factors SOX2 and SOX9, all known to prevent neuronal differentiation (Scott et al., 2010; Ables et al., 2011), was also increased. Consistent with the alteration of the transition between aNSCs and TAPs, we also observed that the *Ptc*-deficient NSCs do not regenerate the SEZ properly after an antimitotic treatment. Nevertheless, our data do not allow excluding the potential existence of additional mechanisms such as, for instance, the alteration of TAP sensitivity to EGF, which would be consistent with the previously reported EGF-mediated induction of TAP proliferation (Doetsch et al., 2002).

Sustained HH signaling activation in the SEZ of deficient mice maintains multipotency but influences the fate of SEZ-derived precursors toward either the oligodendroglial phenotype in the cc or the glutamatergic and dopaminergic phenotypes, two populations of OB periglomerular interneurons, the specification of which may be of high interest in the context of brain repair (Brill et al., 2009; Lledo et al., 2006). The long-lasting high activation of HH signaling is still detected 1 year after the recombination. However, the absence of major alteration of OB morphology we observed in the present work is consistent with previous reports showing that adult neurogenesis in the SEZ allows only a partial turnover of newborn neurons in the OB (Imayoshi et al., 2008; Ninkovic et al., 2007).

Our results point out a likely interaction between HH and NOTCH signaling pathways in adult neurogenesis, suggesting that both should contribute to properly maintain adult NSCs, preventing them to become TAPs (Aguirre et al., 2010; Imayoshi et al., 2013; Kawaguchi et al., 2013). Such

a crosstalk was proposed to be required for the regulation of neurogenic divisions and thus for proper corticogenesis in development (Dave et al., 2011). The constitutive activation of HH signaling through *Ptc* deletion in enteric neural crest cells also robustly activates NOTCH pathway via *Hes1* upregulation and promotes premature gliogenesis, impairing these cells to form ganglia in the hindgut during enteric nervous system development (Ngan et al., 2011). In agreement with HH and NOTCH crosstalk in the adult SEZ, NSCs are both HH (Ahn and Joyner, 2005)- and NOTCH (Aguirre et al., 2010)-responding cells. If HES transcription factors are generally regarded as canonical NOTCH pathway effectors (Imayoshi et al., 2013), a NOTCH-independent HH/HES1 activity was reported in the progenitor cell proliferation of the retina (Wall et al., 2009). We do not know whether *Hes1* is a direct target of HH signaling in the adult NSCs, but our results indicate that the effect of active HH signaling on NSCs is NOTCH dependent. TAPs were reported to regulate NSC self-renewal in vivo, and an interaction between EGFR and NOTCH pathways was proposed to have selective roles in this process with EGFR being an upstream regulator of NOTCH through a nonautonomous mechanism (Aguirre et al., 2010). Because the conditional *Ptc* deletion leads to a huge decrease in EGFR-expressing TAPs in the SEZ, the subsequent EGFR decrease might amplify NOTCH signaling induction and thus also participate in the observed effects. Likewise, SOX9 increase in the conditional *Ptc* mutant is consistent with data reporting that active HH signaling induces *Sox9* transcription and results in the precocious ability of neuroepithelial cells to form neurospheres (Scott et al., 2010).

Despite PTC characterization as a tumor suppressor (Goodrich et al., 1997), we observed that its deletion in astrocyte-like NSCs increases the stemness of these cells without promoting tumor formation. Our data are consistent with the results observed upon the noninducible deletion of *Ptc* in GFAP-expressing NSCs, which was found to promote medulloblastomas only when NSCs have committed to granule neural precursors in the developing cerebellum (Yang et al., 2008). In contrast with the granule precursors, $EGFR^+$ cells that comprise TAPs in the SEZ are not expanding upon *Ptc* deletion. One explanation is that PTC controls a major step of NSC maintenance in the SEZ: the lack of its antagonist activity on SMO results in a blockade of $EGFR^+$ proliferative cells, presumably through increasing NSC symmetric divisions. Further work will have to address if small molecules, positive and negative modulators of SMO that have been developed (Amakye et al., 2013; Gorojankina et al., 2013), also regulate NSC stemness in vivo. Consistent with the present study, recent data have demonstrated that a major decrease in NSC number accounts for the progressive loss of neurogenesis in the SEZ of mice upon conditional ablation of *Smo* in postnatal GFAP-expressing cells (Petrova et al., 2013). By showing the existence of a PTC-mediated activity of SHH in the control of the symmetry or asymmetry of NSC divisions, our data now provide an answer to the question addressed by this study regarding the decision-making process between NSC self-renewal and progenitor generation. Likewise, though ectopic expression of *Gli1* was reported to induce proliferation and transformation of numerous cell types (Dahmane et al., 1997; Nilsson et al., 2000), *Gli1* upregulation is differently interpreted within self-renewing NSC context. Such behavior was previously described in vitro for hippocampus-derived NSCs (Galvin et al., 2008), which upon *Gli1* upregulation, initiate cell-cycle arrest and apoptosis, interpreted as a defense mechanism against hyperproliferation.

As a whole, our work characterized PTC-mediated signals as implicated in the physiological regulation of the generation of NSCs required for sustaining the normal rate of neurogenesis. Instead of promoting precursor cell expansion, *Ptc* deletion was associated with a blockade of $EGFR^+$ proliferating cells, leading to an almost disappearance of neurogenesis while preserving NSCs. Thus, *Glast-CreERT2;Ptc*$^{fl/fl}$ mice should be valuable tools for further investigating molecular regulation and transduction mechanisms associated with NSCs in the SEZ in normal and pathological conditions. These mice should also be of interest for evaluating the effect of PTC in NSC maintenance in the subgranular zone of the hippocampus (Traiffort et al., 2010) and in astroglia (Sirko et al., 2013).

EXPERIMENTAL PROCEDURES

Complete Experimental Procedures are available online (see the Supplemental Experimental Procedures).

Animals

Eight- to 12-week-old animals were used unless indicated. The *Glast-CreERT2* mouse line (Mori et al., 2006) was received on a mixed 129 × C57BL/6 background and backcrossed three times to C57BL/6. The *Ptc* floxed/floxed mouse line (Uhmann et al., 2007) was received and maintained on C57BL/6 background. The reporter mouse line *R26R-YFP/+* was a gift from Drs. F. Costantini and T.M. Jessell (Srinivas et al., 2001) kept on C57Bl/6 background. The *Glast-CreERT2* mouse line was crossed to the *Ptc* floxed/floxed mouse line. The progeny was then crossed to *R26R-YFP/+* mice genotyped as described by Soriano (1999). All procedures were carried out according to the European Communities Council Directive (86/806/EEC) and protocols approved by Institutional Animal Care and Use Committee.

Tamoxifen and BrdU Administration

Tamoxifen (Sigma-Aldrich) was dissolved in corn oil (Sigma-Aldrich) at 10 mg/ml, and 1 mg was injected intraperitoneally (i.p.) twice a day for 5 consecutive days. Animals were killed 10 days, or 2, 6, or 12 months after the end of tamoxifen

application. In order to label fast proliferating cells, mice received an i.p. injection of BrdU (Sigma-Aldrich; 100 mg/kg of body weight) 4 and 2 hr before sacrifice (n = 5–6/group). For the determination of cell-cycle exit, animals received two BrdU i.p. injections at 2 hr intervals and were sacrificed 24 hr after the last injection.

Osmotic Minipump Infusion

To kill all fast proliferating cells in the SEZ, AraC (2%; Sigma-Aldrich) in vehicle (0.9% saline) was infused into the lateral ventricles in control and $Ptc^{-/-}$ mice that had been injected with tamoxifen 6 months earlier. We used miniosmotic pumps (ALZET). After 7 days of infusion, the pumps were removed, and mice were killed 10 days after the end of AraC infusion (n = 4 per condition). Cannulas were implanted stereotaxically into the lateral ventricle at the following coordinates: anteroposterior, 0.2 mm; mediolateral, 0.8 mm; and dorsoventral, −2.5 mm (relative to bregma).

SUPPLEMENTAL INFORMATION

Supplemental Information includes Supplemental Experimental Procedures and six figures and can be found with this article online at http://dx.doi.org/10.1016/j.stemcr.2014.05.016.

ACKNOWLEDGMENTS

We thank Professor M. Götz (Helmholtz Zentrum, Munich) for generously providing us with the *Glast-CreERT2*, Drs. P. Brulet and S. Picaud (NED, Gif/Yvette) for providing the initial breeding mice, and Professor T. Jessell (Columbia University) for *R26R-YFP/+* mouse lines. We thank Professor O. Kiehn and Drs. L. Borgius and J. Bouvier (Karolinska Institute, Stockholm) for providing us with the *vGlut2* probe. We are very grateful to E. Desale and T. Durand (TAAM, CNRS-UPS44, Orléans) for excellent technical assistance. LY411575 was obtained as a gift from Chemical Synthesis Core Facility (Mayo Clinic Jacksonville, Jacksonville). J.F. is supported in part by fellowships from the Direction Générale des Armées, the Association pour la Recherche sur le Cancer, and CNRS. This work was supported by the French Agence Nationale de la Recherche (Grant 07-physio-010-04 to E.T.) and La Ligue contre le Cancer, Comité de l'Essonne (n°M20632) et des Yvelines and Fondation ARC (n°20131200300 to M.R.).

Received: February 24, 2014
Revised: May 22, 2014
Accepted: May 22, 2014
Published: June 19, 2014

REFERENCES

Ables, J.L., Breunig, J.J., Eisch, A.J., and Rakic, P. (2011). Not(ch) just development: Notch signalling in the adult brain. Nat. Rev. Neurosci. *12*, 269–283.

Aguirre, A., Rubio, M.E., and Gallo, V. (2010). Notch and EGFR pathway interaction regulates neural stem cell number and self-renewal. Nature *467*, 323–327.

Ahn, S., and Joyner, A.L. (2005). In vivo analysis of quiescent adult neural stem cells responding to Sonic hedgehog. Nature *437*, 894–897.

Amakye, D., Jagani, Z., and Dorsch, M. (2013). Unraveling the therapeutic potential of the Hedgehog pathway in cancer. Nat. Med. *19*, 1410–1422.

Angot, E., Loulier, K., Nguyen-Ba-Charvet, K.T., Gadeau, A.P., Ruat, M., and Traiffort, E. (2008). Chemoattractive activity of sonic hedgehog in the adult subventricular zone modulates the number of neural precursors reaching the olfactory bulb. Stem Cells *26*, 2311–2320.

Balordi, F., and Fishell, G. (2007). Mosaic removal of hedgehog signaling in the adult SVZ reveals that the residual wild-type stem cells have a limited capacity for self-renewal. J. Neurosci. *27*, 14248–14259.

Bidet, M., Joubert, O., Lacombe, B., Ciantar, M., Nehmé, R., Mollat, P., Brétillon, L., Faure, H., Bittman, R., Ruat, M., and Mus-Veteau, I. (2011). The hedgehog receptor patched is involved in cholesterol transport. PLoS ONE *6*, e23834.

Brill, M.S., Ninkovic, J., Winpenny, E., Hodge, R.D., Ozen, I., Yang, R., Lepier, A., Gascón, S., Erdelyi, F., Szabo, G., et al. (2009). Adult generation of glutamatergic olfactory bulb interneurons. Nat. Neurosci. *12*, 1524–1533.

Briscoe, J., and Thérond, P.P. (2013). The mechanisms of Hedgehog signalling and its roles in development and disease. Nat. Rev. Mol. Cell Biol. *14*, 416–429.

Chen, J.K., Taipale, J., Young, K.E., Maiti, T., and Beachy, P.A. (2002). Small molecule modulation of Smoothened activity. Proc. Natl. Acad. Sci. USA *99*, 14071–14076.

Colak, D., Mori, T., Brill, M.S., Pfeifer, A., Falk, S., Deng, C., Monteiro, R., Mummery, C., Sommer, L., and Götz, M. (2008). Adult neurogenesis requires Smad4-mediated bone morphogenic protein signaling in stem cells. J. Neurosci. *28*, 434–446.

Costa, M.R., Ortega, F., Brill, M.S., Beckervordersandforth, R., Petrone, C., Schroeder, T., Götz, M., and Berninger, B. (2011). Continuous live imaging of adult neural stem cell division and lineage progression in vitro. Development *138*, 1057–1068.

Dahmane, N., Lee, J., Robins, P., Heller, P., and Ruiz i Altaba, A. (1997). Activation of the transcription factor Gli1 and the Sonic hedgehog signalling pathway in skin tumours. Nature *389*, 876–881.

Dave, R.K., Ellis, T., Toumpas, M.C., Robson, J.P., Julian, E., Adolphe, C., Bartlett, P.F., Cooper, H.M., Reynolds, B.A., and Wainwright, B.J. (2011). Sonic hedgehog and notch signaling can cooperate to regulate neurogenic divisions of neocortical progenitors. PLoS ONE *6*, e14680.

Doetsch, F., Petreanu, L., Caille, I., Garcia-Verdugo, J.M., and Alvarez-Buylla, A. (2002). EGF converts transit-amplifying neurogenic precursors in the adult brain into multipotent stem cells. Neuron *36*, 1021–1034.

Fauq, A.H., Simpson, K., Maharvi, G.M., Golde, T., and Das, P. (2007). A multigram chemical synthesis of the gamma-secretase inhibitor LY411575 and its diastereoisomers. Bioorg. Med. Chem. Lett. *17*, 6392–6395.

Galvin, K.E., Ye, H., Erstad, D.J., Feddersen, R., and Wetmore, C. (2008). Gli1 induces G2/M arrest and apoptosis in hippocampal but not tumor-derived neural stem cells. Stem Cells *26*, 1027–1036.

Gonzalez-Perez, O., and Alvarez-Buylla, A. (2011). Oligodendrogenesis in the subventricular zone and the role of epidermal growth factor. Brain Res. Brain Res. Rev. *67*, 147–156.

Goodrich, L.V., Milenković, L., Higgins, K.M., and Scott, M.P. (1997). Altered neural cell fates and medulloblastoma in mouse patched mutants. Science *277*, 1109–1113.

Gorojankina, T., Hoch, L., Faure, H., Roudaut, H., Traiffort, E., Schoenfelder, A., Girard, N., Mann, A., Manetti, F., Solinas, A., et al. (2013). Discovery, molecular and pharmacological characterization of GSA-10, a novel small-molecule positive modulator of Smoothened. Mol. Pharmacol. *83*, 1020–1029.

Ihrie, R.A., Shah, J.K., Harwell, C.C., Levine, J.H., Guinto, C.D., Lezameta, M., Kriegstein, A.R., and Alvarez-Buylla, A. (2011). Persistent sonic hedgehog signaling in adult brain determines neural stem cell positional identity. Neuron *71*, 250–262.

Imayoshi, I., Sakamoto, M., Ohtsuka, T., Takao, K., Miyakawa, T., Yamaguchi, M., Mori, K., Ikeda, T., Itohara, S., and Kageyama, R. (2008). Roles of continuous neurogenesis in the structural and functional integrity of the adult forebrain. Nat. Neurosci. *11*, 1153–1161.

Imayoshi, I., Shimojo, H., Sakamoto, M., Ohtsuka, T., and Kageyama, R. (2013). Genetic visualization of notch signaling in mammalian neurogenesis. Cell. Mol. Life Sci. *70*, 2045–2057.

Karpowicz, P., Willaime-Morawek, S., Balenci, L., DeVeale, B., Inoue, T., and van der Kooy, D. (2009). E-Cadherin regulates neural stem cell self-renewal. J. Neurosci. *29*, 3885–3896.

Kawaguchi, D., Furutachi, S., Kawai, H., Hozumi, K., and Gotoh, Y. (2013). Dll1 maintains quiescence of adult neural stem cells and segregates asymmetrically during mitosis. Nat Commun *4*, 1880–1892.

Kazanis, I., Lathia, J.D., Vadakkan, T.J., Raborn, E., Wan, R., Mughal, M.R., Eckley, D.M., Sasaki, T., Patton, B., Mattson, M.P., et al. (2010). Quiescence and activation of stem and precursor cell populations in the subependymal zone of the mammalian brain are associated with distinct cellular and extracellular matrix signals. J. Neurosci. *30*, 9771–9781.

Lledo, P.M., Alonso, M., and Grubb, M.S. (2006). Adult neurogenesis and functional plasticity in neuronal circuits. Nat. Rev. Neurosci. *7*, 179–193.

Machold, R., Hayashi, S., Rutlin, M., Muzumdar, M.D., Nery, S., Corbin, J.G., Gritli-Linde, A., Dellovade, T., Porter, J.A., Rubin, L.L., et al. (2003). Sonic hedgehog is required for progenitor cell maintenance in telencephalic stem cell niches. Neuron *39*, 937–950.

Marshall, C.A.G., Novitch, B.G., and Goldman, J.E. (2005). Olig2 directs astrocyte and oligodendrocyte formation in postnatal subventricular zone cells. J. Neurosci. *25*, 7289–7298.

Mori, T., Tanaka, K., Buffo, A., Wurst, W., Kühn, R., and Götz, M. (2006). Inducible gene deletion in astroglia and radial glia—a valuable tool for functional and lineage analysis. Glia *54*, 21–34.

Ngan, E.S., Garcia-Barceló, M.M., Yip, B.H., Poon, H.C., Lau, S.T., Kwok, C.K., Sat, E., Sham, M.H., Wong, K.K., Wainwright, B.J., et al. (2011). Hedgehog/Notch-induced premature gliogenesis represents a new disease mechanism for Hirschsprung disease in mice and humans. J. Clin. Invest. *121*, 3467–3478.

Nilsson, M., Undèn, A.B., Krause, D., Malmqwist, U., Raza, K., Zaphiropoulos, P.G., and Toftgård, R. (2000). Induction of basal cell carcinomas and trichoepitheliomas in mice overexpressing GLI-1. Proc. Natl. Acad. Sci. USA *97*, 3438–3443.

Ninkovic, J., Mori, T., and Götz, M. (2007). Distinct modes of neuron addition in adult mouse neurogenesis. J. Neurosci. *27*, 10906–10911.

Pastrana, E., Silva-Vargas, V., and Doetsch, F. (2011). Eyes wide open: a critical review of sphere-formation as an assay for stem cells. Cell Stem Cell *8*, 486–498.

Petrova, R., Garcia, A.D., and Joyner, A.L. (2013). Titration of GLI3 repressor activity by sonic hedgehog signaling is critical for maintaining multiple adult neural stem cell and astrocyte functions. J. Neurosci. *33*, 17490–17505.

Ponti, G., Obernier, K., and Alvarez-Buylla, A. (2013). Lineage progression from stem cells to new neurons in the adult brain ventricular-subventricular zone. Cell Cycle *12*, 1649–1650.

Roudaut, H., Traiffort, E., Gorojankina, T., Vincent, L., Faure, H., Schoenfelder, A., Mann, A., Manetti, F., Solinas, A., Taddei, M., and Ruat, M. (2011). Identification and mechanism of action of the acylguanidine MRT-83, a novel potent Smoothened antagonist. Mol. Pharmacol. *79*, 453–460.

Ruat, M., Roudaut, H., Ferent, J., and Traiffort, E. (2012). Hedgehog trafficking, cilia and brain functions. Differentiation *83*, S97–S104.

Scott, C.E., Wynn, S.L., Sesay, A., Cruz, C., Cheung, M., Gomez Gaviro, M.V., Booth, S., Gao, B., Cheah, K.S., Lovell-Badge, R., and Briscoe, J. (2010). SOX9 induces and maintains neural stem cells. Nat. Neurosci. *13*, 1181–1189.

Shook, B.A., Manz, D.H., Peters, J.J., Kang, S., and Conover, J.C. (2012). Spatiotemporal changes to the subventricular zone stem cell pool through aging. J. Neurosci. *32*, 6947–6956.

Sirko, S., Behrendt, G., Johansson, P.A., Tripathi, P., Costa, M., Bek, S., Heinrich, C., Tiedt, S., Colak, D., Dichgans, M., et al. (2013). Reactive glia in the injured brain acquire stem cell properties in response to sonic hedgehog. [corrected]. Cell Stem Cell *12*, 426–439.

Soriano, P. (1999). Generalized lacZ expression with the ROSA26 Cre reporter strain. Nat. Genet. *21*, 70–71.

Srinivas, S., Watanabe, T., Lin, C.S., William, C.M., Tanabe, Y., Jessell, T.M., and Costantini, F. (2001). Cre reporter strains produced by targeted insertion of EYFP and ECFP into the ROSA26 locus. BMC Dev. Biol. *1*, 4–11.

Traiffort, E., Angot, E., and Ruat, M. (2010). Sonic Hedgehog signaling in the mammalian brain. J. Neurochem. *113*, 576–590.

Uhmann, A., Dittmann, K., Nitzki, F., Dressel, R., Koleva, M., Frommhold, A., Zibat, A., Binder, C., Adham, I., Nitsche, M., et al. (2007). The Hedgehog receptor Patched controls lymphoid lineage commitment. Blood *110*, 1814–1823.

Wall, D.S., Mears, A.J., McNeill, B., Mazerolle, C., Thurig, S., Wang, Y., Kageyama, R., and Wallace, V.A. (2009). Progenitor cell proliferation in the retina is dependent on Notch-independent Sonic hedgehog/Hes1 activity. J. Cell Biol. *184*, 101–112.

Yang, Z.J., Ellis, T., Markant, S.L., Read, T.A., Kessler, J.D., Bourboulas, M., Schüller, U., Machold, R., Fishell, G., Rowitch, D.H., et al. (2008). Medulloblastoma can be initiated by deletion of Patched in lineage-restricted progenitors or stem cells. Cancer Cell *14*, 135–145.

Stem Cell Reports, Volume *3*

Supplemental Information

Genetic Activation of Hedgehog Signaling Unbalances the Rate of Neural Stem Cell Renewal by Increasing Symmetric Divisions

Julien Ferent, Loïc Cochard, Hélène Faure, Maurizio Taddei, Heidi Hahn, Martial Ruat, and Elisabeth Traiffort

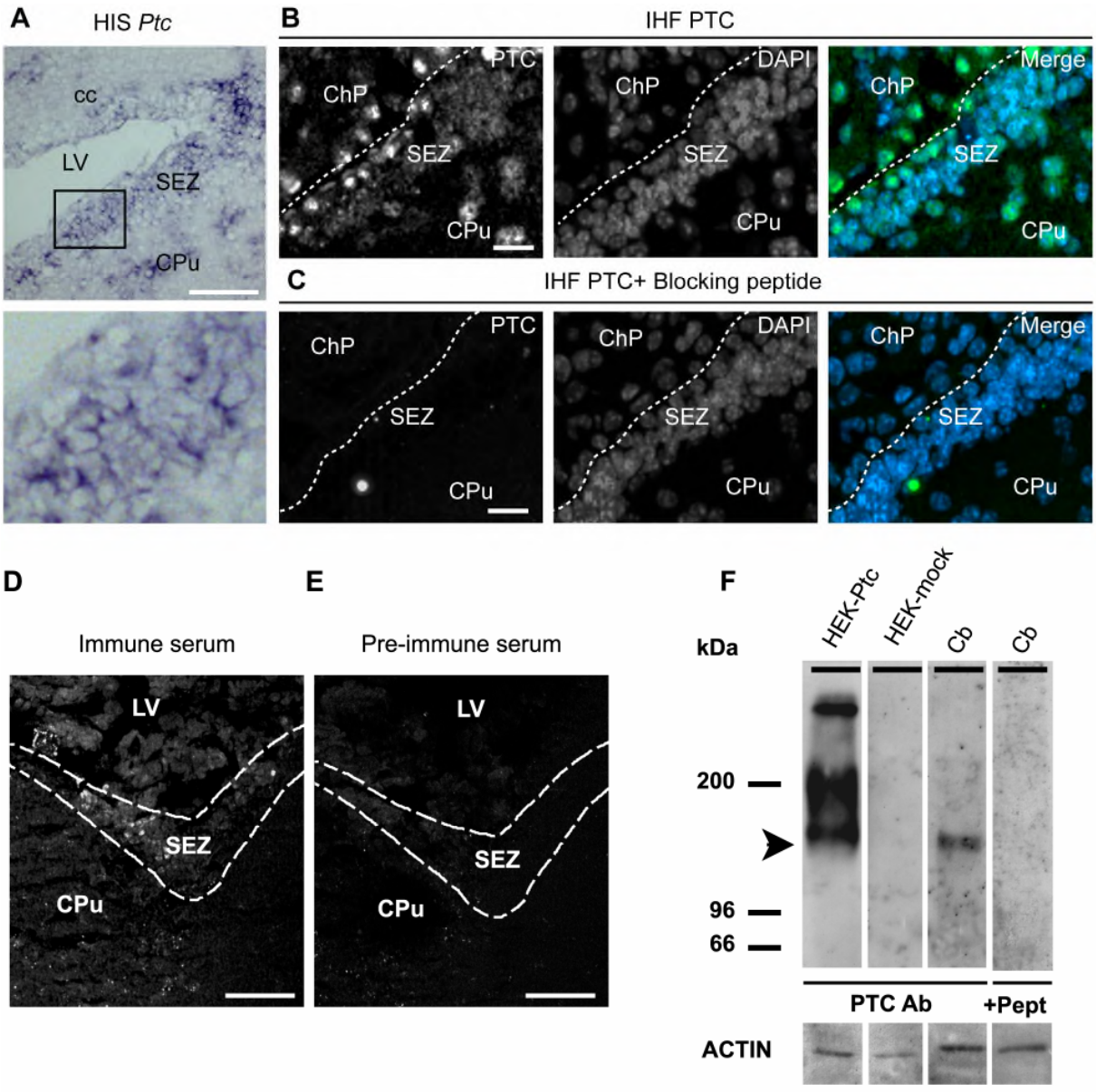
A
HIS Ptc
cc
LV
SEZ
CPu
B
IHF PTC
PTC
ChP
SEZ
CPu
DAPI
ChP
SEZ
CPu
Merge
ChP
SEZ
CPu
C
IHF PTC+ Blocking peptide
PTC
ChP
SEZ
CPu
DAPI
ChP
SEZ
CPu
Merge
ChP
SEZ
CPu
D
Immune serum
LV
SEZ
CPu
E
Pre-immune serum
LV
SEZ
CPu
F
HEK-Ptc
HEK-mock
Cb
Cb
kDa
200
96
66
PTC Ab
+Pept
ACTIN

Figure S1

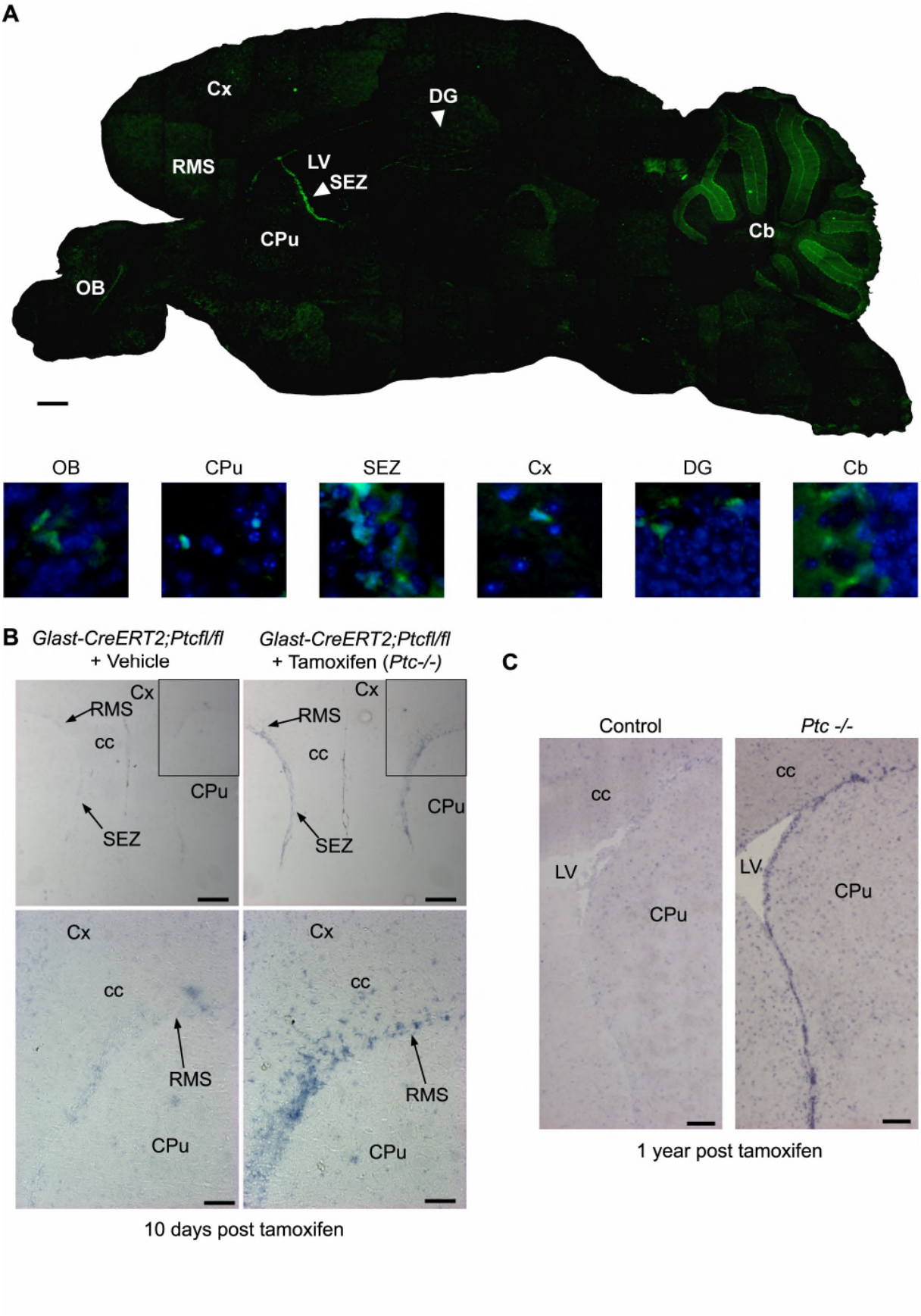
A
Cx
DG
RMS
LV
SEZ
CPu
Cb
OB
OB
CPu
SEZ
Cx
DG
Cb
B
Glast-CreERT2;Ptcfl/fl
+ Vehicle
Glast-CreERT2;Ptcfl/fl
+ Tamoxifen (Ptc-/-)
Cx
RMS
cc
CPu
SEZ
Cx
RMS
cc
CPu
SEZ
Cx
cc
RMS
CPu
Cx
cc
RMS
CPu
10 days post tamoxifen
C
Control
Ptc -/-
cc
LV
CPu
cc
LV
CPu
1 year post tamoxifen

Figure S2

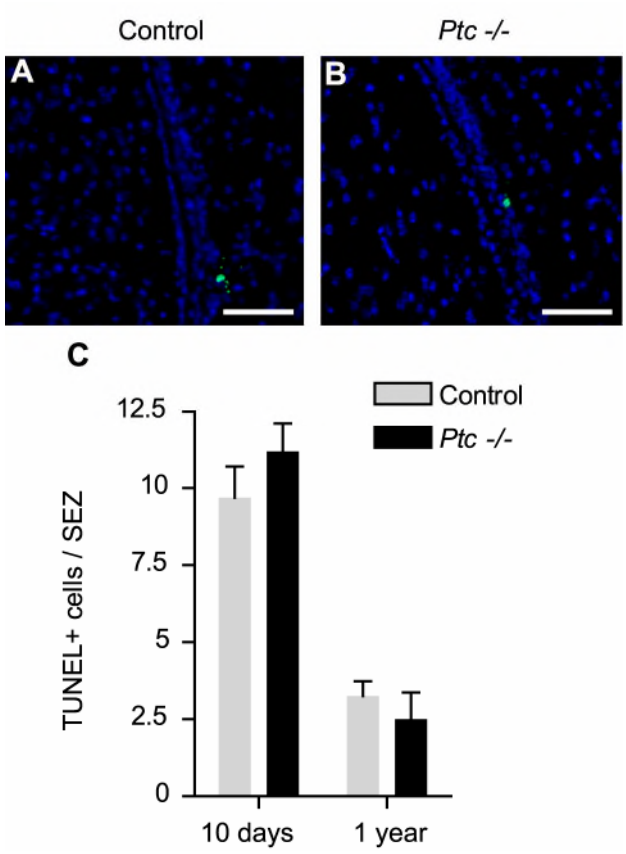
Control
Ptc -/-
A
B
C
Control
Ptc -/-
TUNEL+ cells / SEZ
12.5
10
7.5
5
2.5
0
10 days
1 year

Figure S3

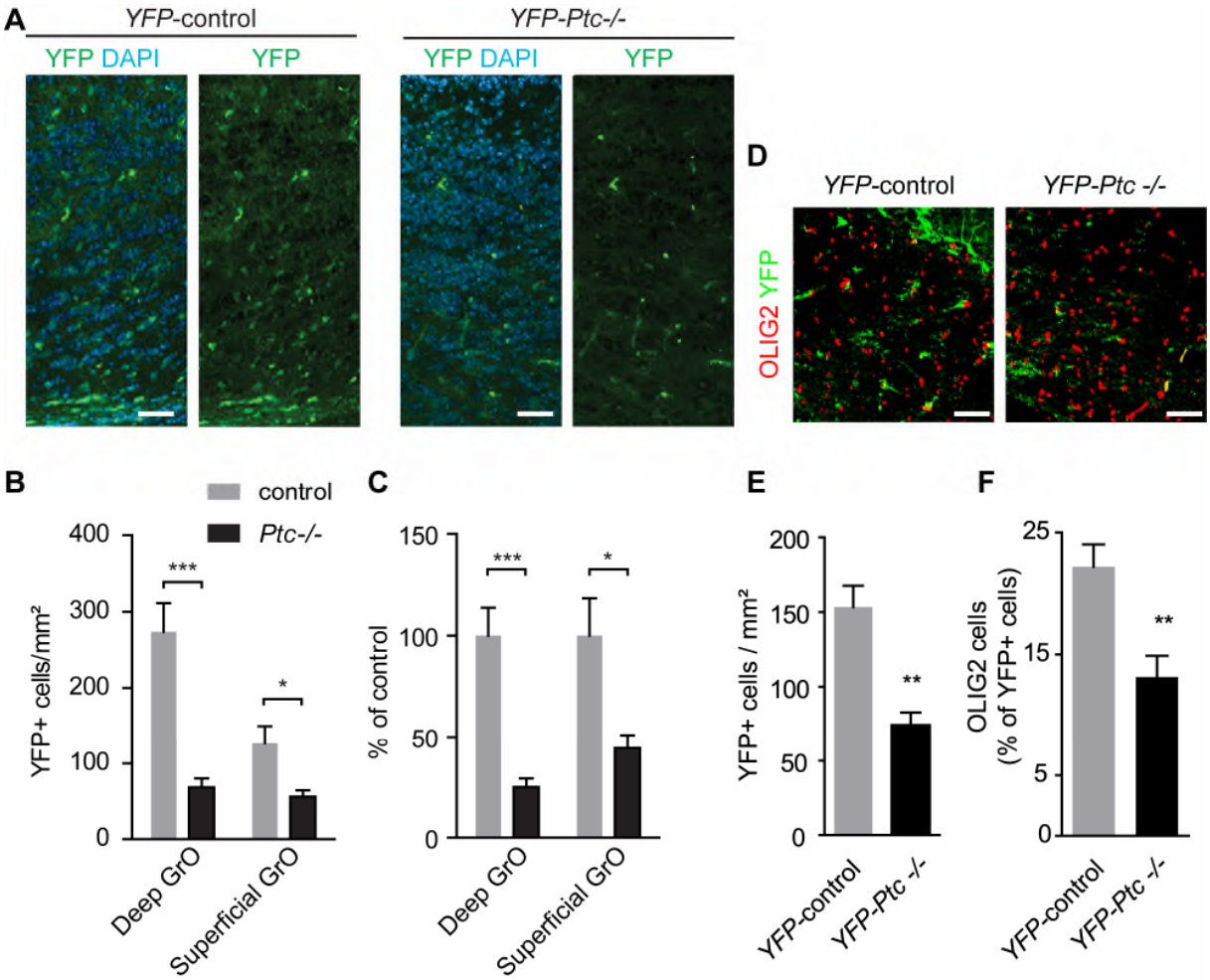
A
YFP-control
YFP-Ptc-/-
YFP DAPI
YFP
YFP DAPI
YFP
D
YFP-control
YFP-Ptc -/-
OLIG2 YFP
B
control
Ptc-/-
YFP+ cells/mm²
400
300
200
100
0
***
*
Deep GrO
Superficial GrO
C
% of control
150
100
50
0
***
*
Deep GrO
Superficial GrO
E
YFP+ cells / mm²
200
150
100
50
0
**
YFP-control
YFP-Ptc -/-
F
OLIG2 cells
(% of YFP+ cells)
25
15
5
0
**
YFP-control
YFP-Ptc -/-

Figure S4

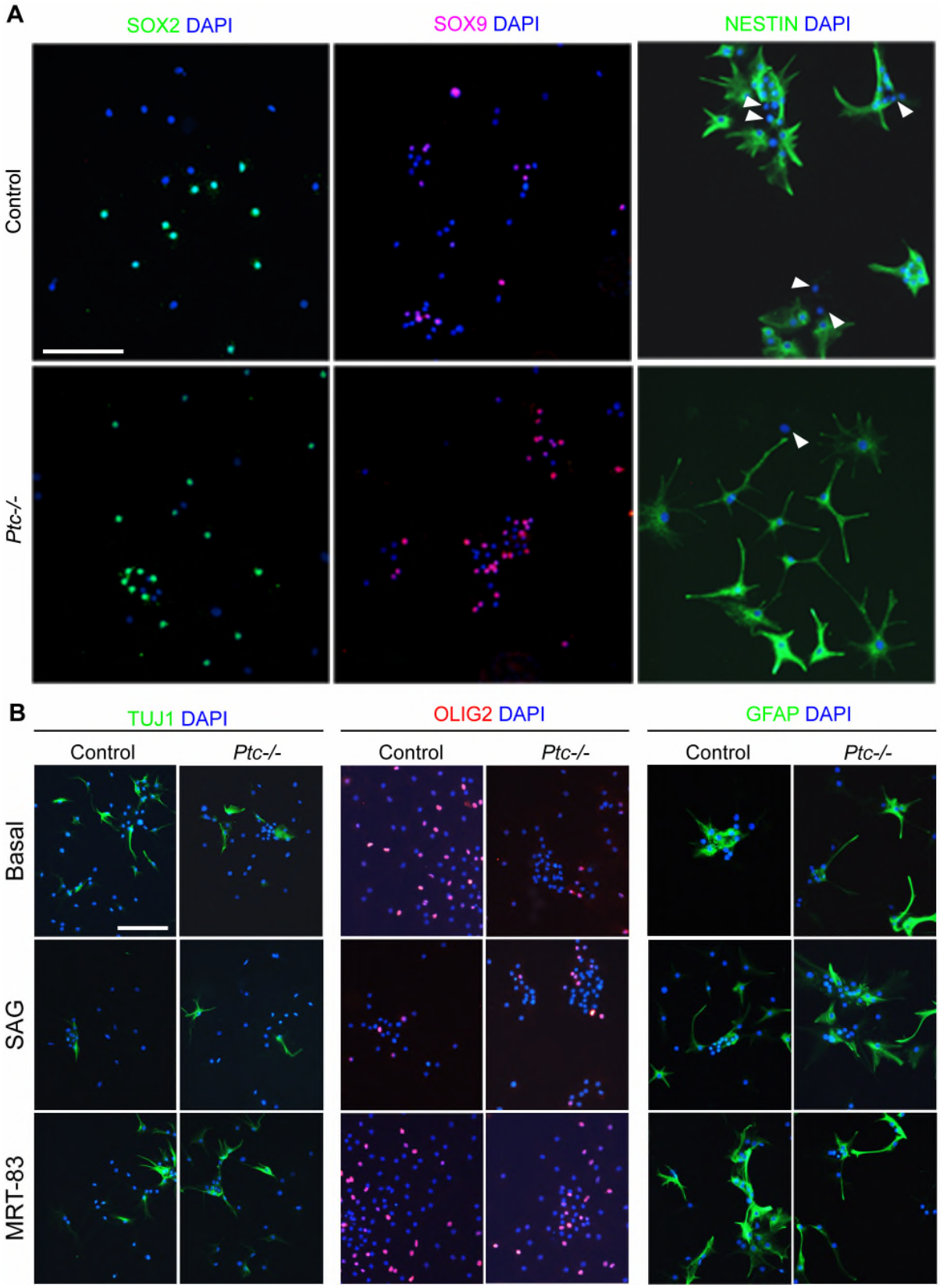
A
SOX2 DAPI
SOX9 DAPI
NESTIN DAPI
Control
Ptc-/-
B
TUJ1 DAPI
OLIG2 DAPI
GFAP DAPI
Control
Ptc-/-
Control
Ptc-/-
Control
Ptc-/-
Basal
SAG
MRT-83

Figure S5

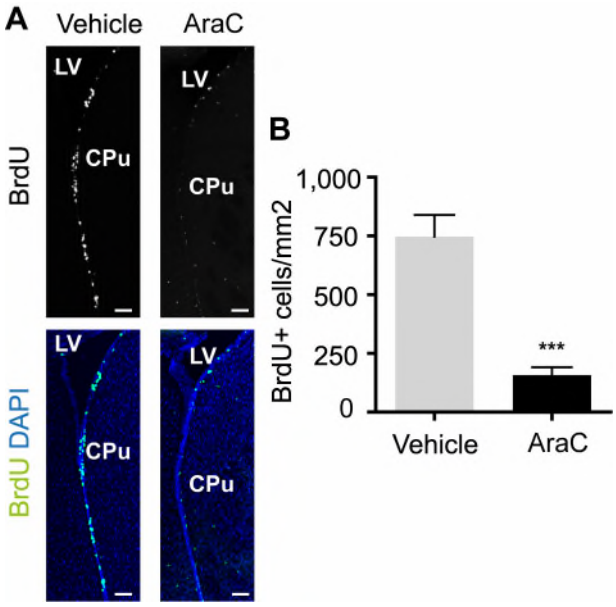
A
Vehicle
AraC
LV
CPu
BrdU
BrdU DAPI
B
BrdU+ cells/mm2
1,000
750
500
250
0
***
Vehicle
AraC

Figure S6

Figure S1. Expression of PTC in the adult SEZ, Related to Figure 1. (A), *In situ* hybridization of *Ptc* transcripts in the dorsal SEZ. The bottom panel is a magnification of the boxed area. (B,C), IHF staining performed at the level of the dorsal SEZ using the polyclonal Ab130 PTC antiserum in the absence (B) or in the presence (C) of the fusion protein used for antibody production. Signals associated to PTC^+ cells are observed in the SEZ, but are absent in preadsorption experiments. **(**D,E). IHF staining performed at the level of the SEZ using the polyclonal Ab130 PTC antiserum identified signals associated to PTC^+ cells that were not evidenced when the experiments were performed with the corresponding pre-immune serum. (F), Immunoblot analysis of whole cell lysates (4 µg of proteins) from HEK293 cells transiently transfected with an empty vector (mock) or with a vector containing the full length DNA encoding mouse PTC was performed by SDS-PAGE using the PTC antiserum Ab130. The arrowhead indicates a major band of 140 kDa detected in HEK-PTC but not in HEK-mock. A second signal of 200 kDa is also detected in HEK-PTC and might reflect post-translational modifications. P5 cerebellum (Cb) proteins (30 µg) were analyzed using the same PTC antiserum leading to a signal of 140 kDa which is blocked in preadsorption experiments. Abbreviations: ChP, choroid plexus; CPu, caudate putamen. Scale bars (µm): 100 (A, D, E); 25 (B, C).

Figure S2. Characterization of Cre-mediated recombination in the newly generated transgenic mouse lines, Related to Figure 1. (A) *YFP*-control animals received tamoxifen for 5 days and were analyzed 2 months after induction. Successful recombination was monitored by direct visualization of YFP fluorescence. Bottom panels are magnifications of the indicated region. (B) ISH performed with the *Gli1* riboprobe on slices derived from *Glast-CreERT2/*$Ptc^{fl/fl}$ animals treated by vehicle (left) or tamoxifen (right; $Ptc^{-/-}$) 10 days before analysis. Induction of the target gene *Gli1* is detected upon tamoxifen but not vehicle

treatment. The boxed areas are magnified in the corresponding bottom panels. (C) *Gli1* up-regulation is still strongly detected in slices derived from *Ptc*$^{-/-}$ and control mice treated with tamoxifen 1 year before. Abbreviations: Cb, cerebellum; cc, corpus callosum; CPu, caudate putamen; Cx, cerebral cortex; DG, dentate gyrus; LV, lateral ventricle; OB, olfactory bulb; RMS, rostral migratory stream; SEZ, subependymal zone. Scale bars (µm); 500 (A), 400 (B, top), 200 (C), 100 (B, bottom).

Figure S3. Conditional *Ptc* deletion in GLAST^{+} cells of the SEZ does not modify cell apoptosis, Related to Figure 2. Detection of TUNEL^{+} nuclei in the SEZ of control (A) or *Ptc*$^{-/-}$ (B) animals and quantification (C) of these nuclei 10 days and 1 year after tamoxifen injection. Data are mean ± SEM from 3-4 animals. Scale bars: 100µm.

Figure S4. Recombination in OB granular cells and oligodendroglial lineage, Related to Figure 3. (A) Visualization of the YFP reporter in the superficial (top) and deep (bottom) granular layers of the OB in *YFP*-control and *YFP-Ptc*$^{-/-}$ mice. (B,C) Histograms showing the quantification of YFP^{+} cells expressed as cell number / mm^{2} (B) and as percentage of YFP^{+} cells quantified in *YFP*-control animals (total number of counted cells, n=223 for *YFP*-control, n=73 for *YFP-Ptc*$^{-/-}$). (D) OLIG2 IHF performed at the level of the corpus callosum (cc) of *YFP*-control and *YFP-Ptc*$^{-/-}$ mice. YFP-expressing cells likely correspond to both endogenous astrocytes expressing GLAST and the progeny of GLAST^{+} NSC born in the SEZ which have migrated and undergone differentiation into cells of the oligodendroglial lineage. (E,F), Histograms showing the quantification of the density of YFP^{+} cells (E) and the percentage of YFP^{+} cells which co-express OLIG2 in *YFP*-control and *YFP-Ptc*$^{-/-}$ cc (total number of counted cells, n= 187 for *YFP*-control, n= 74 for *YFP-Ptc*$^{-/-}$). Values are the mean ± SEM from 3-4 animals. *, p≤0.05, **, p≤0.01, ***, p≤0.005 Scale bars : 50 µm.

Figure S5. Visualization of SEZ-derived cell cultures from control and *Ptc*$^{-/-}$ mice, Related to Figure 4. (A) IHF using SOX2, SOX9 and NESTIN antibodies are performed on control (top) and *Ptc*$^{-/-}$ (bottom) precursor cell cultures maintained in the absence of growth factors for 12 h before the experiment. Nuclei are labeled with DAPI (blue). (B) IHF using TUJ1, OLIG2 and GFAP antibodies are performed on control (left) or *Ptc*$^{-/-}$ (right) precursor cell cultures maintained in the absence of growth factors for 7 days before the experiment in the presence or in the absence of the HH agonist SAG (0.3 µM) and HH antagonist MRT-83 (3 µM). Nuclei are labeled with DAPI (blue). Scale bars: 100µm.

Figure S6. Depletion of BrdU-incorporating cells in the SEZ of wild-type mice, Related to Figure 6. (A), Coronal views of the SEZ showing BrdU-incorporating cells (top) together with DAPI^{+} nuclei (bottom) at the end of AraC or vehicle infusion (t=0) in wild–type mice. (B), Quantification of BrdU^{+} cells indicates a marked reduction in cell proliferation. Values are the mean ± SEM from 3 animals. ***, $p \leq 0.0001$. Scale bars: 200µm.

Supplemental experimental procedures

Histology and immunostaining. Animals were or not perfused by 4% paraformaldehyde and tissue sections were sectioned using a cryostat. Antibodies were as follows: BrdU, GFAP, NEUN, PSA-NCAM, β-GAL as described in (Angot et al., 2008), goat C-FOS (1/300; Santa Cruz), mouse KI67 (1/300; BD Pharmingen), guinea pig GLAST (1/100; Millipore), mouse NESTIN (1/500; Millipore), rabbit OLIG2 (1/1000; Millipore), rabbit EGFR (1/400; Millipore), rabbit SOX2 (1/400; Millipore), goat SOX9 (1/400; R&D Systems), mouse TUJ1 (1/500; Abcam), rabbit calbindin (1/500, Swant). The secondary antibodies were goat anti-mouse Alexa 546 (Molecular Probes), goat anti-rabbit Alexa 555 (Life Technologies), donkey anti-goat Alexa 546 (Life Technologies), goat anti-mouse FITC (Sigma), anti-guinea pig

DyLight 488 (Jackson immunoresearch), goat anti-rat Alexa 488 (Jackson Immunoresearch), biotinylated goat anti-rat (Vector Laboratories), donkey anti-mouse, -goat or -rabbit DyLight 649 conjugated antibodies (Jackson Immunoresearch). Cell nuclei were visualized using DAPI (Vector). TUNEL analysis was performed by using Terminal deoxynucleotidyl transferase dUTP nick-end labeling (TUNEL) experiments (ApoptagR Peroxidase In situ Apoptosis Detection Kit; Millipore) according to supplier's protocol. For hematoxylin and eosin staining, hematoxilin (Vector) and eosin (Polysciences) were applied.

***In situ* hybridization.** ISH protocol and synthesis of *Ptc*, *Gli1* and *Gfap* specific riboprobes were as previously described (Traiffort et al., 1999). *Ptc del* riboprobe corresponds to mouse *Ptc* nucleotides 1025-1305 (Genbank accession NM_008957.2). The *vGlut2* probe was a kind gift from Dr O. Kiehn (Borgius et al., 2010).

Neurosphere cultures. The telencephalic SEZ was dissected from adult wild-type, $Ptc^{-/-}$ or control animals (Pastrana et al., 2011). SEZ fragments were digested in papain (Sigma) and trypsin (Invitrogen) solution for 20 min at 37°C and mechanically dissociated by passing through a 26-gauge needle. If not stated otherwise, single cells were seeded at 5000 cells per well in 24-well plates in serum-free media consisting of DMEM supplemented with B27, penicillin/streptomycin, sodium pyruvate and in the presence of 20 ng/ml EGF and 10 ng/ml basic fibroblast growth factor (FGF, Invitrogen). After 6–9 d in cultures, spheres were collected, incubated in 0.05% Trypsin (Invitrogen) for 30–60 min at 37°C, mechanically dissociated and reseeded as single cells as described above. If not indicated otherwise, the cells were derived from animals treated 2 months earlier with tamoxifen and the experiments involving single cells or neurospheres (either treated with drugs or untreated) were performed after one or two passages or on primary spheres.

For the multipotency experiments, 5-10 spheres were cultured on poly-D-lysine (Sigma) coated coverslips in the above mentioned medium devoid of growth factors for 7 days. For the immunofluorescence studies, cells were fixed in 4% PFA at 4°C for 30 min, before blocking for 30 min at room temperature in 0.5% BSA in PBS. The fixed cells were then incubated with the primary antibodies at room temperature for 90 min, followed by incubation with secondary antibodies for 60 min and mounting of the coverslips.

For the paired cell assay, single cells were plated directly after SVZ microdissection on coated coverslips at a cell density of about 50,000 cells per well. The cultures were maintained for 24-36 h in the presence of 10 ng/ml of EGF. IHF analyses were performed as described above. About 60 pairs were evaluated in each mutant and wild type sample.

The labeling index allowing the evaluation of the cell cycle length corresponds to the percentage of $KI67^{+}$ precursors that were labeled by a single pulse of BrdU. The dissociated spheres were cultured on poly-d-lysine coated coverslips in the presence of growth factors, treated with 10 µM BrdU for the indicated time frames and processed further for anti-BrdU and KI67 IHF.

Drugs. SAG and MRT-83 were synthesized as described (Roudaut et al., 2011).

Semi-quantitative RT-PCR. Total RNA was isolated using the Trizol kit (Invitrogen) from sphere cultures derived from animals treated with tamoxifen 2 months before. RNA was reverse transcribed in 20 µl reactions with Superscript II reverse transcriptase (Invitrogen). PCR reactions were performed using Go Taq polymerase (Promega). *Actin* was used to assess input RNA levels. The sequences of the primers which were used are as follows:

Notch1, Fwd: 5'CCAGCATGGCCAGCTCTGG3'

Rev: 5'CATCCAGATCTGTGGCCCTGTT3'

Hes1, Fwd: 5'AAAGACGGCCTCTGAGCACA3'

Rev: 5'TCATGGCGTTGATCTGGGTCA3'

Hes5, Fwd: 5'AAGTACCGTGGCGGTGGAGATGC3'

Rev: 5'CGCTGGAAGTGGTAAAGCAGCTT3'

Gli1, Fwd: 5'TTCGTGTGCCATTGGGGAGG3'

Rev: 5'CTTGGGCTCCACTGTGGAGA3'

Western blot analysis

Cerebellum from P5 OF1 mice (Charles Rivers, Saint-Germain sur l'Arbresle, France) were homogenized. Proteins derived from the pellet obtained after a 20 min centrifugation at 9000 g were electrophoresed on 8% polyacrylamide gels as described previously (Coulombe et al., 2004). Immunoreactivity was detected using the polyclonal antiserum (130Ab, 1:1000; Bidet et al., 2011) to the mouse PTC. Blocking experiments were performed by overnight preincubation of the antiserum with the recombinant mouse glutathione-S-transferase (GST)–PTC purified fusion protein (15 µg/ml).

Quantification and statistical analysis. Immunofluorescent signals were detected by a conventional epifluorescence microscope (DMRXA2; Leica Microsystems) equipped with a CDD camera (Photometrics) or scanned for Z stacks colocalizations by an Apotome micoscope (ZEISS) and AxioImager software. Optical sections were set as 1 µm intervals. Cells displaying an immunoreactive or ISH signal and areas were quantified using ImageJ software. Cell counts are presented as an average of several SEZ or olfactory bulb slices from at least three different mice per group. Statistical analysis was performed using the unpaired bilateral Student's t test. Statistical significance was considered for $p<0.05$.

Supplemental references

Angot, E., Loulier, K., Nguyen-Ba-Charvet, K. T., Gadeau, A. P., Ruat, M., and Traiffort, E. (2008) Chemoattractive activity of sonic hedgehog in the adult subventricular zone modulates the number of neural precursors reaching the olfactory bulb. Stem cells *26*, 2311-2320.

Bidet, M., Joubert, O., Lacombe, B., Ciantar, M., Nehme, R., Mollat, P., Bretillon, L., Faure, H., Bittman, R., Ruat, M., Mus-Veteau, I. (2011) The hedgehog receptor patched is involved in cholesterol transport. PloS one *6*, e23834.

Borgius, L., Restrepo, C.E., Leao, R.N., Saleh, N., and Kiehn, O. (2010) A transgenic mouse line for molecular genetic analysis of excitatory glutamatergic neurons. Mol. Cell. Neurosci. *45*, 245-257.

Coulombe, J., Traiffort, E., Loulier, K., Faure, H. and Ruat, M. (2004) Hedgehog interacting protein in the mature brain: membrane-associated and soluble forms. Mol. Cell. Neurosci. *25*, 323-333.

Pastrana, E., Silva-Vargas, V. and Doetsch, F. (2011) Eyes wide open: a critical review of sphere-formation as an assay for stem cells. Cell Stem Cell *8*, 486-498.

Roudaut, H., Traiffort, E., Gorojankina, T., Vincent, L., Faure, H., Schoenfelder, A., Mann, A., Manetti, F., Solinas, A., Taddei, M., and Ruat M. (2011) Identification and mechanism of action of the acylguanidine MRT-83, a novel potent Smoothened antagonist. Mol. Pharmacol. *79*, 453-460.

Traiffort, E., Charytoniuk, D., Watroba, L., Faure, H., Sales, N., and Ruat, M. (1999) Discrete localizations of hedgehog signalling compotents in the developing and adult rat nervous system. Eur. J. Neurosci. *11*, 3199-3214.